PHILOSOPHICAL TRANSACTIONS OF THE ROYAL SOCIETY A MATHEMATICAL, PHYSICAL & ENGINEERING SCIENCES

Pattern Selection with Anisotropy during Directional Solidification

R. B. Hoyle, G. B. McFadden and S. H. Davis

Phil. Trans. R. Soc. Lond. A 1996 **354**, 2915-2949
doi: 10.1098/rsta.1996.0135

Pattern selection with anisotropy during directional solidification

By R. B. Hoyle[1], G. B. McFadden[2] and S. H. Davis[1]

[1] *Department of Engineering Sciences and Applied Mathematics, McCormick School of Engineering and Applied Science, Northwestern University, Evanston, IL 60208, USA*

[2] *Computing and Applied Mathematics Laboratory, National Institute of Standards and Technology, Gaithersburg, MD 20899, USA*

Contents

The effects of surface-tension anisotropy on interface morphology during the directional solidification of a binary alloy are studied. The long-wave evolution equation derived by Brattkus & Davis to describe growth near the absolute stability limit is generalized to include the effects of a surface tension with cubic anisotropy. The special cases of growth in the [001], [011] and [111] directions are considered. The resulting evolution equations are derived, and amplitude equations governing roll/rectangle and roll/hexagon competition are obtained. The coefficients of the amplitude equations depend on the surface-tension anisotropy, and determine how pattern selection is influenced by the presence of geometrically preferred directions. Anisotropy leads to changes in the existence and stability criteria for each pattern, to imperfect bifurcations, and to loss of degeneracy in bifurcations.

Phil. Trans. R. Soc. Lond. A (1996) **354**, 2915–2949
Printed in Great Britain

1. Introduction

When a binary alloy is solidified, the microstructures that appear, e.g. cells, dendrites, and eutectics, depend on the processing conditions, the composition of the alloy, and the crystallographic orientation. For example, Morris & Winegard (1969) studied cellular growth in lead-antimony alloys and found that at the onset of instability the interface morphology depends on the crystallographic orientation. When the growth direction is near [100] or [111], nodes are formed, while near the [011] direction, two-dimensional cells (rolls) emerge. The fact that for a cubic crystal different morphologies arise when different growth directions are imposed suggests that the agent responsible for these differences is an anisotropic interfacial property.

Anisotropy due to the presence of crystalline structure can take many forms. The bulk materials properties can display directional variations. For example, Coriell *et al.* (1990) studied how anisotropic thermal conductivities in a uniaxial crystal affect the morphological stability of the solid–liquid interface. They found that, depending on the growth direction, stationary or travelling rolls are the preferred morphologies at the onset of instability. The solid–liquid interface can display kinetic effects in which the undercooling is related to the pulling speed. The proportionality factor, the kinetic coefficient, can have directional properties that give rise to travelling waves on the front in a linear theory, as shown by Coriell & Sekerka (1976), and hence the appearance at finite amplitude of cells tilted with respect to the pulling direction, as shown by Young *et al.* (1987). Finally, the surface energy γ can have directional properties. For example, if the crystal has four-fold symmetry about a given axis, then

$$\gamma = \gamma_0(1 + \epsilon_4 \cos 4\hat{\theta}) \tag{1.1}$$

is a typical model for the dependence of surface energy on the angle $\hat{\theta}$ between the interface normal and a specific direction for a two-dimensional interface lying in a symmetry plane of the crystal; here γ_0 and ϵ_4 are constants. When ϵ_4 is very small, then one might expect that such anisotropies would have negligible effects. However, they are essential to the existence of two-dimensional needle dendrites according to microscopic solvability theory (Langer 1987). When ϵ_4 is larger, certain orientations are forbidden, and crystals with corners form (Herring 1951; Voorhees *et al.* 1984).

There have been direct measurements of surface-tension anisotropy; a recent review of measurements for several materials used in dendritic-growth experiments is given by Muschol *et al.* 1992. Glicksman & Singh (1986) found that pure succinonitrile has an anisotropy ϵ_4 of 0.5%, and Muschol *et al.* (1992) found a similar value of $0.55 \pm 0.15\%$. For pivalic acid there are larger discrepancies in the measured values. For pure pivalic acid Glicksman & Singh (1989) found an anisotropy ϵ_4 of 5%, while Muschol *et al.* (1992) found a smaller value of $2.5 \pm 0.2\%$. Measurements of pivalic acid with 1% ethanol were made by Dougherty (1991), who found a relatively small anisotropy of $0.6 \pm 0.2\%$, which would suggest a substantial variation of the anisotropy with the addition of ethanol, whereas Muschol *et al.* (1992) find a value of $2.6 \pm 0.2\%$, which shows little sensitivity to the addition of ethanol.

There is a great deal of theory devoted to the nonlinear development of interfacial perturbations in directional solidification. The first weakly nonlinear analysis was performed by Wollkind & Segel (1970). These theories use as their point of departure the linear theory of Mullins & Sekerka (1964), and explore extensions into the weakly nonlinear regime, as summarized by Coriell & McFadden (1993). Questions

of preferred pattern, preferred length scale, and bifurcation structure (sub- or supercritical bifurcation) have been investigated. There are, however, two points that make the story incomplete. On the one hand, nearly the whole low-speed branch of the neutral curve of linear theory (near the constitutional supercooling limit) in two dimensions involves subcritical bifurcations, and so jump transitions to cellular structures are predicted. The cells that emerge cannot be described accurately by linear theory. One consequence of this is that the cellular scales of two-dimensional experiments (de Cheveigné *et al.* 1988) and theory (Mullins & Sekerka 1964) do not agree to better than a factor of two. On the other hand, nearly all of the theories include the effects of processing parameters and the composition of the alloy, but ignore effects of the presence of the crystalline structure, in particular the anisotropies in surface energy. An exception is McFadden *et al.* (1988), in which a three-dimensional weakly nonlinear theory is begun and taken through quadratic terms in amplitude. A transcritical bifurcation to hexagons is found, though the branch is unstable. They cannot describe the large-amplitude branch to which the unstable disturbances tend because it is generally outside the weakly nonlinear regime.

In the present work we attempt to remedy the two deficiencies outlined above. Firstly, we shall focus on the high-speed branch of the neutral curve (near absolute stability) where two-dimensional cells bifurcate supercritically and so can be described by a weakly nonlinear theory. Rather than attack the primitive equations involving a free-boundary problem for the interface, we analyse the strongly nonlinear evolution equation of Brattkus & Davis (1988) that for high speeds is asymptotically equivalent to the original problem. By this means, the pattern-selection problem becomes tractable. Secondly, we introduce surface-energy anisotropy, focusing on growth of a cubic material in the [100], [111] and [011] directions, and delve into the question of how the patterns change as the magnitude of the anisotropy increases from zero. We first study the competition between two sets of rolls with an angle θ between them. Superposition of the rolls leads to solutions with square or rectangular planforms, patterns which have been observed in other physical systems (see, for example, Hoyle 1993, and references therein). We then consider the competition of three rolls aligned at 120° to one another in order to further examine the effect of anisotropy on the selection of hexagons.

The consideration of these elementary nonlinear interactions is one simplification. Another is that, even though we examine the high-speed branch of instabilities, we ignore kinetic effects (Coriell & Sekerka 1976) produced by non-equilibrium thermodynamics at the interface. Further, the thermal field is assumed to be a fixed linear function of distance from the unperturbed solid–liquid interface. In this approximation the thermal conductivities of the liquid and solid are assumed equal, and the effects of the release of latent heat at the solidifying interface are neglected. The effects of relaxing this simplifying assumption on a long-wave theory have been considered by Huntley & Davis (1993), who examine the low-wavenumber end of the neutral curve under a variety of conditions.

In this paper, the long-wave evolution equation derived by Brattkus & Davis (1988) is first generalized to include the effects of anisotropic surface energy; a generalized equation results for each of the three growth directions considered. These long-wave evolution equations are the starting point for a bifurcation analysis of rectangular and hexagonal patterns in the presence of anisotropy. The anisotropy is found to affect linear pattern selection in the [011] case, and nonlinear selection in the [100] and [111] cases. Anisotropy leads to changes in the existence and stability criteria for each

PHILOSOPHICAL TRANSACTIONS OF THE ROYAL SOCIETY A MATHEMATICAL, PHYSICAL & ENGINEERING SCIENCES

pattern, to imperfect bifurcations, and to loss of degeneracy in bifurcations. Since the various anisotropic properties of the solid are all dictated by the basic symmetries of the underlying crystal lattice, we expect the results we obtain from consideration of surface-tension anisotropy to be typical of other types of anisotropic properties as well. Although derived in the context of directional solidification, the amplitude equations which describe the bifurcation structure are more generally applicable to anisotropic pattern-forming systems, for example, electrohydrodynamic convection of nematic liquid crystals.

2. Model

We use the model of surface-tension anisotropy considered by McFadden *et al.* (1988). The Gibbs–Thomson equation with anisotropic surface energy may be written in the form,

$$T_{\mathrm{I}} = T_{\mathrm{M}} + mc - T_{\mathrm{M}}\mathcal{E}/L_{\mathrm{V}}, \tag{2.1}$$

where T_{I} is the interface temperature, T_{M} is the bulk melting point of the pure material, m is the liquidus slope, c is the solute concentration, $\mathcal{E}$ is the the *weighted mean curvature* (Taylor 1992), and L_{V} is the latent heat per unit volume. (The densities of the liquid and solid are assumed to be equal.) $\mathcal{E}$ reduces to the product of the surface energy with twice the mean curvature in the case of isotropic surface energy.

The anisotropic form for $\mathcal{E}$ can be calculated from a variational principle involving the surface energy. In general the anisotropic surface energy is a function of the unit normal $\boldsymbol{n}$ to the solid–liquid interface $z = h(x, y, t)$. Here z is the coordinate in the growth direction, and x and y are coordinates in the orthogonal plane. Because we are concerned with the evolution of interfaces that remain single-valued, it is more convenient for our purposes to write the dependence on orientation in the equivalent form $\gamma = \gamma(h_x, h_y)$, since the normal can be given in terms of the interface gradient by

$$\boldsymbol{n} \equiv (n_x, n_y, n_z) = (-h_x, -h_y, 1)/\sqrt{1 + h_x^2 + h_y^2}.$$

The weighted mean curvature can then be derived by taking the variation of the expression (McFadden *et al.* 1988)

$$\int I(h_x, h_y)\,\mathrm{d}x\mathrm{d}y \equiv \int \gamma(h_x, h_y)\sqrt{1 + h_x^2 + h_y^2}\,\mathrm{d}x\mathrm{d}y \tag{2.2}$$

to obtain

$$\delta \int I(h_x, h_y)\,\mathrm{d}x\mathrm{d}y = \int \mathcal{E}\delta h\,\mathrm{d}x\mathrm{d}y, \tag{2.3}$$

where

$$-\mathcal{E} = I_{11}h_{xx} + 2I_{12}h_{xy} + I_{22}h_{yy}, \tag{2.4}$$

and the subscripts on I denote partial derivatives with

$$I_{11} = \frac{\partial^2 I(h_x, h_y)}{\partial(h_x)^2}, \qquad I_{12} = \frac{\partial^2 I(h_x, h_y)}{\partial(h_x)\partial(h_y)}, \qquad I_{22} = \frac{\partial^2 I(h_x, h_y)}{\partial(h_y)^2}. \tag{2.5}$$

For the isotropic case $\gamma(h_x, h_y) = \bar{\gamma}$, where $\bar{\gamma}$ is constant; this results in $\mathcal{E} = \bar{\gamma}\mathcal{K}$, where $\mathcal{K}$ is twice the mean curvature.

For the purposes of a weakly nonlinear expansion, it suffices to work with a low-order expansion of I in terms of h_x and h_y. In a coordinate system aligned with the crystalline axes, the surface energy $\gamma(n_x, n_y, n_z)$, being defined on the unit sphere, can be expressed as an expansion in spherical harmonics with cubic symmetry, or equivalently

$$\gamma(n_x, n_y, n_z) = \gamma'_0 + \gamma'_4(n_x^4 + n_y^4 + n_z^4) + \gamma'_6(n_x^6 + n_y^6 + n_z^6) + \dots \tag{2.6}$$

Transforming to a frame with the z axis aligned along the growth direction, and writing $(n_x, n_y, n_z) = (-h_x, -h_y, 1)/(1 + h_x^2 + h_y^2)^{1/2}$ and $I(h_x, h_y) = (1 + h_x^2 + h_y^2)^{1/2}\gamma(h_x, h_y)$, we find that for growth in the [100], [111] or [011] directions, the function I can be expanded in the form,

$$I(h_x, h_y) = \tfrac{1}{2}\bar{\gamma}_1 h_x^2 + \tfrac{1}{2}\bar{\gamma}_2 h_y^2 + \bar{\gamma}_3 h_x(h_x^2 - 3h_y^2) + \bar{\gamma}_4 h_x^4 + \bar{\gamma}_5 h_x^2 h_y^2 + \bar{\gamma}_6 h_y^4 + O(|\nabla h|^5), \tag{2.7}$$

where we have omitted inconsequential constant or linear terms that do not contribute to $\mathcal{E}$, and where the $\bar{\gamma}_i$ are linear combinations of the γ'_j (McFadden *et al.* 1988).

The inclusion of surface-tension anisotropy modifies the long-wave evolution equation derived by Brattkus & Davis (1988). In their treatment the primitive equations are rendered dimensionless by using the length scale D/V and time scale D/V^2, where D is the solute diffusivity and V is the pulling velocity. The solute concentration, c, is made dimensionless in terms of the scale $(k-1)c_\infty/k$, where $k > 0$ is the distribution coefficient and c_∞ is the far-field solute concentration. This introduces three dimensionless parameters (Brattkus & Davis 1988), given by k, the morphological parameter M, defined by

$$M = \frac{m(k-1)c_\infty V}{kGD}, \tag{2.8}$$

where G is the temperature gradient (assumed constant), and the scaled surface energy

$$\Gamma = \frac{kT_{\mathrm{M}}V(\bar{\gamma}_1/L_{\mathrm{V}})}{c_\infty m(k-1)D}, \tag{2.9}$$

which is based on the constant $\bar{\gamma}_1$ defined in (2.7). The dimensionless form of the quantity I has the form,

$$I(h_x, h_y) = \tfrac{1}{2}h_x^2 + \tfrac{1}{2}\gamma_2 h_y^2 + \gamma_3 h_x(h_x^2 - 3h_y^2) + \gamma_4 h_x^4 + \gamma_5 h_x^2 h_y^2 + \gamma_6 h_y^4 + O(|\nabla h|^5), \tag{2.10}$$

where h is now dimensionless, and we have introduced $\gamma_2 = \bar{\gamma}_2/\bar{\gamma}_1$, $\gamma_3 = \bar{\gamma}_3/\bar{\gamma}_1$, $\gamma_4 = \bar{\gamma}_4/\bar{\gamma}_1$, $\gamma_5 = \bar{\gamma}_5/\bar{\gamma}_1$, and $\gamma_6 = \bar{\gamma}_6/\bar{\gamma}_1$.

In the presence of anisotropic surface-tension, the dimensionless equations governing the evolution of the solute concentration, and the interface position are

$$\nabla^2 c + c_{zz} + c_z = c_t, \quad z > 0, \tag{2.11 a}$$

$$[1 + (k-1)c](1 + h_t) = c_z - \nabla h \cdot \nabla c, \quad z = h, \tag{2.11 b}$$

$$c - M^{-1}h - \Gamma\mathcal{E} = 0, \quad z = h, \tag{2.11 c}$$

$$c = 1, \quad z = \infty, \tag{2.11 d}$$

where $\nabla \equiv (\partial_x, \partial_y)$ is the two-dimensional gradient operator. The base state, corresponding to a flat interface, is given by $h = 0$, $c = 1 - \mathrm{e}^{-z}$.

3. Linear stability

Surface-tension anisotropy affects the conditions for linear stability of the base state. For the case of growth in an arbitrary fixed direction, the linear stability results generally depend on both the magnitude and direction of the perturbation wavevector. The dispersion relation for a perturbation of growth rate σ and wavevector (a_1, a_2) is given by

$$\sigma = -k + (1 - M^{-1} - \Gamma a_1^2 - \gamma_2 \Gamma a_2^2)[(\tfrac{1}{4} + \sigma + a_1^2 + a_2^2)^{1/2} + k - \tfrac{1}{2}]. \tag{3.1}$$

For growth in some special directions, for example [100] and [111], it is found that $\gamma_2 = 1$ (McFadden *et al.* 1988), and the dispersion relation of linear theory depends only on the magnitude, and not the direction, of the wavevector. Growth in the [100] or the [111] direction therefore gives rise to interesting weakly nonlinear problems in nonlinear pattern selection. Growth in directions for which $\gamma_2 \neq 1$ is dominated by linear selection at small amplitudes.

The neutral stability surface is given by $\sigma = 0$, and the marginal stability condition can be determined by finding the global maximum of M^{-1} on the neutral stability surface. The stationary points of M^{-1} are given by

$$\frac{\partial M^{-1}}{\partial a_1} = -2\Gamma a_1 + \frac{a_1 k}{(\frac{1}{4} + a_1^2 + a_2^2)^{1/2}[(\frac{1}{4} + a_1^2 + a_2^2)^{1/2} + k - \frac{1}{2}]^2} = 0, \tag{3.2a}$$

$$\frac{\partial M^{-1}}{\partial a_2} = -2\gamma_2 \Gamma a_2 + \frac{a_2 k}{(\frac{1}{4} + a_1^2 + a_2^2)^{1/2}[(\frac{1}{4} + a_1^2 + a_2^2)^{1/2} + k - \frac{1}{2}]^2} = 0. \tag{3.2b}$$

The origin $a_1 = a_2 = 0$ is a stationary point, as is the point $a_1 = 0$, $a_2 = a_{20}$, where

$$2\gamma_2 \Gamma(\tfrac{1}{4} + a_{20}^2)^{1/2}[(\tfrac{1}{4} + a_{20}^2)^{1/2} + k - \tfrac{1}{2}]^2 - k = 0, \tag{3.3}$$

and $a_2 = 0$, $a_1 = a_{10}$, where

$$2\Gamma(\tfrac{1}{4} + a_{10}^2)^{1/2}[(\tfrac{1}{4} + a_{10}^2)^{1/2} + k - \tfrac{1}{2}]^2 - k = 0. \tag{3.4}$$

If $\Gamma < 0$ or $\gamma_2 \Gamma < 0$, then $M^{-1} \to +\infty$ in some direction as a_1^2, $a_2^2 \to \infty$. This is obviously the global maximum of M^{-1}, and short waves become unstable first. For $\Gamma > 0$ and $\gamma_2 \Gamma > 0$ there are four possibilities. If $1/k - \Gamma < 0$ and $1/k - \gamma_2 \Gamma < 0$ there are no instabilities. If $1/k - \Gamma < 0$ and $1/k - \gamma_2 \Gamma > 0$, the global maximum is at $a_1 = 0$, $a_2 = a_{20}$, and stability is first lost to a y-roll at finite wavelength. If $1/k - \Gamma > 0$ and $1/k - \gamma_2 \Gamma < 0$, then the global maximum is at $a_1 = a_{10}$, $a_2 = 0$, and stability is first lost to finite-wavelength x-rolls. If $1/k - \Gamma > 0$ and $1/k - \gamma_2 \Gamma > 0$ then either finite-wavelength x- or y-rolls are most unstable, depending on the heights of the respective maxima of M^{-1}. In the special case where $\Gamma = \Gamma\gamma_2$, the maxima are of equal height, and there is no preferred direction for the most unstable mode, only a critical overall wavenumber, a_0.

In the work of Brattkus & Davis (1988), a long-wave evolution equation for the interface shape is derived for growth near conditions of absolute stability. From the above analysis, it can be seen that the absolute stability boundary is given by $\Gamma = 1/k$ and $\gamma_2 \Gamma = 1/k$. For growth directions where $\gamma_2 = 1$, e.g. [100] and [111], a small parameter ϵ is introduced by setting $\Gamma = \gamma_2 \Gamma = 1/k - \epsilon$. In most directions, however, $\gamma_2 \neq 1$, and in order to derive the modified Brattkus–Davis equation, we must set $\Gamma = 1/k - \epsilon$ and $\gamma_2 = 1 + \tilde{\gamma}_2 \epsilon$. Examination of the dispersion relation in the limit $\epsilon \ll 1$ then indicates (Brattkus & Davis 1988) that disturbances have wavenumbers

PHILOSOPHICAL TRANSACTIONS OF THE ROYAL SOCIETY A MATHEMATICAL, PHYSICAL & ENGINEERING SCIENCES

that are $O(\epsilon^{1/2})$ and have time scales that are $O(1/\epsilon)$; the morphological parameter M scales as $O(1/\epsilon^2)$. This motivates the scalings $\bar{M} = \epsilon^2 M$, $h(x, y, t) = H(X, Y, \tilde{T})$, where $(X, Y) = \epsilon^{1/2}(x, y)$, and $\tilde{T} = \epsilon t$. This gives

$$-\mathcal{E} = \epsilon\{I_{11}(\epsilon^{1/2}H_X, \epsilon^{1/2}H_Y)H_{XX} + 2I_{12}(\epsilon^{1/2}H_X, \epsilon^{1/2}H_Y)H_{XY} + I_{22}(\epsilon^{1/2}H_X, \epsilon^{1/2}H_Y)H_{YY}\}. \quad (3.5)$$

For I, as given in equation (2.10), the appropriate form of the small-ϵ expansion for $\mathcal{E}$ is affected by the cubic term proportional to γ_3, since this term introduces a factor of $\epsilon^{1/2}$ that does not occur in the isotropic case.

The modified Brattkus–Davis equations are derived by expanding c and H in powers of ϵ (Brattkus & Davis 1988). For growth in the [100] direction, we have $\tilde{\gamma}_2 = 0$, $\tilde{\gamma}_3 = 0$ and $\gamma_4 = \gamma_6$ (McFadden *et al.* 1988), and the equation is found to be

$$\begin{aligned} &F_{\tau\tau} - \nabla^2 F_\tau + \tfrac{1}{4}(1-\nu^2)\nabla^4 F + \nabla^2 F + \mu^{-1} F \\ &\quad = F_\tau \nabla^2 F + |\nabla F|^2_\tau - \tfrac{1}{2}(1-\nu)\nabla^2(|\nabla F|^2) - \nu\nabla\cdot(\nabla F \nabla^2 F) \\ &\qquad + 4\gamma_4 \nabla\cdot\{|\nabla F|^2 \nabla F\} + 2(\gamma_5 - 2\gamma_4)[F_\eta^2 F_{\xi\xi} + 4F_\eta F_\xi F_{\xi\eta} + F_\xi^2 F_{\eta\eta}], \end{aligned} \quad (3.6)$$

where

$$F = \frac{k}{2k+1} H^{(0)}, \quad (3.7\,a)$$

$$(\xi, \eta) = \frac{k^{3/2}}{2k+1}(X, Y), \quad (3.7\,b)$$

$$\tau = \frac{k^2}{2k+1}\tilde{T}, \quad (3.7\,c)$$

$$\nu = \frac{1}{2k+1}, \quad (3.7\,d)$$

$$\mu^{-1} = \frac{(2k+1)^2}{k^3}\bar{M}^{-1}. \quad (3.7\,e)$$

In this case, there is four-fold symmetry in the ξ–η plane, and the ξ and η directions lie along two of the crystalline axes, as shown in figure 1*a*.

For growth in the [111] direction, we have $\tilde{\gamma}_2 = 0$, $\tilde{\gamma}_3 \neq 0$, $\gamma_4 = -\frac{1}{8} + O(\epsilon^{1/2})$, $\gamma_5 = -\frac{1}{4} + O(\epsilon^{1/2})$ and $\gamma_6 = -\frac{1}{8} + O(\epsilon^{1/2})$ (McFadden *et al.* 1988), and the equation is

$$\begin{aligned} &F_{\tau\tau} - \nabla^2 F_\tau + \tfrac{1}{4}(1-\nu^2)\nabla^4 F + \nabla^2 F + \mu^{-1} F \\ &\quad = F_\tau \nabla^2 F + |\nabla F|^2_\tau - \tfrac{1}{2}(1-\nu)\nabla^2(|\nabla F|^2) - \nu\nabla\cdot(\nabla F \nabla^2 F) \\ &\qquad - \tfrac{1}{2}\nabla\cdot\{|\nabla F|^2 \nabla F\} + \hat{\gamma}_3[F_\xi F_{\xi\xi} - 2F_\eta F_{\xi\eta} - F_\xi F_{\eta\eta}], \end{aligned} \quad (3.8)$$

where $\hat{\gamma}_3 = 6\gamma_3/k^{1/2}\epsilon^{1/2}$. Now there is three-fold symmetry in the ξ–η plane, and the ξ direction lies along one of the three symmetry axes, while the η direction lies perpendicular to this axis, as illustrated in figure 1*b*.

The marginal stability condition for growth in both the [100] and [111] directions is

$$\tfrac{1}{4}(1-\nu^2)a^4 - a^2 + \mu^{-1} = 0, \quad (3.9)$$

where a is the modulus of the wavenumber of the perturbation. The critical wavenumber a_c is then given by

$$a_c^2 = \frac{2}{1-\nu^2}, \quad (3.10)$$

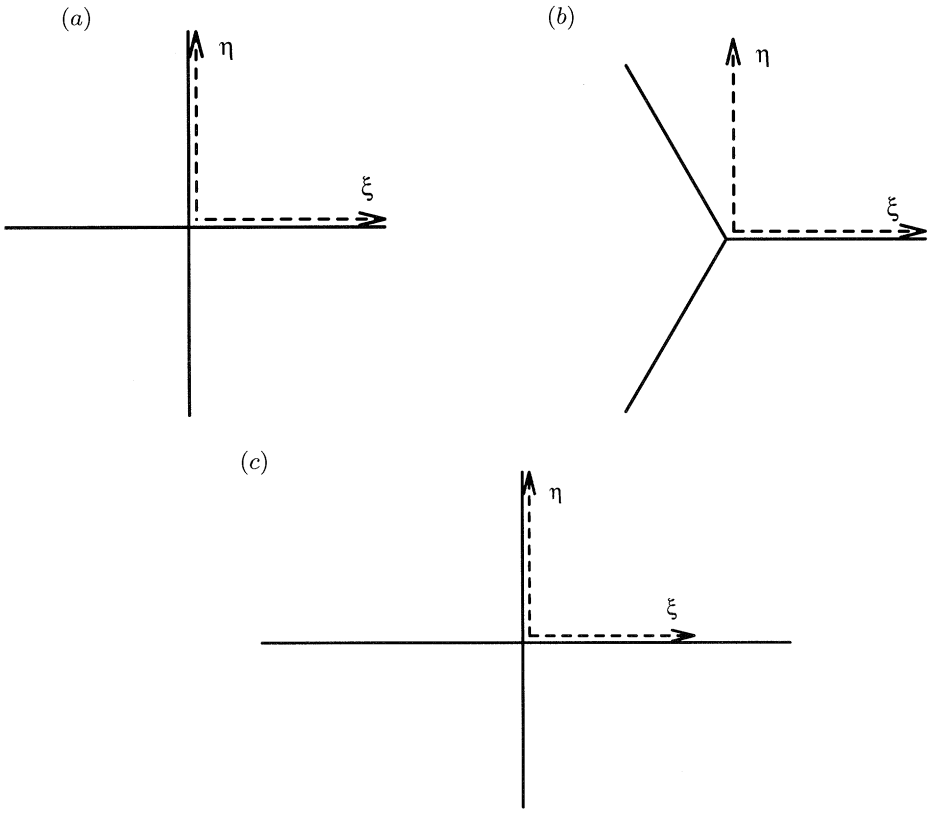

Figure 1. (*a*) For growth in the [100] direction, the ξ and η axes (dashed lines) lie along two of the crystalline axes (solid lines). (*b*) When growth is in the [111] direction, there is three-fold symmetry in the ξ–η plane. The ξ direction (dashed line) lies along one of the three symmetry axes (solid lines), while the η direction (dashed line) lies perpendicular to this axis. (*c*) For solidification in the [110] direction, there is two-fold symmetry in the ξ–η plane; there are two perpendicular symmetry axes (solid lines), but they are not equivalent (indicated here by the different lengths of the two lines). The ξ direction (dashed line) lies along one of the symmetry axes, which is also one of the crystalline axes, while the η direction (dashed line) lies along the other symmetry axis. The direction of solidification is directly out of the plane of the paper.

and the critical value μ_c is given by

$$\mu_c^{-1} = \frac{1}{1-\nu^2}. \tag{3.11}$$

We recall that $\nu = 1/(1+2k)$, where $k > 0$ is the distribution coefficient, so that $0 < \nu < 1$. The critical wavenumber thus lies in the range $2 < a_c^2 < \infty$ as k ranges over the interval $0 < k < \infty$.

For the [011] direction, we have $\tilde{\gamma}_3 = 0$ (McFadden *et al.* 1988), and the modified Brattkus–Davis equation is

$$\begin{aligned} &F_{\tau\tau} - \nabla^2 F_\tau + \tfrac{1}{4}(1-\nu^2)\nabla^4 F + \nabla^2 F + \mu^{-1} F - \frac{2\nu\tilde{\gamma}_2}{1-\nu} F_{\eta\eta} \\ &\quad = F_\tau \nabla^2 F + |\nabla F|_\tau^2 - \tfrac{1}{2}(1-\nu)\nabla^2(|\nabla F|^2) - \nu\nabla\cdot(\nabla F \nabla^2 F) \\ &\qquad + 4\gamma_4 (F_\xi^3)_\xi + 4\gamma_6 (F_\eta^3)_\eta + 2\gamma_5 (F_\xi^2 F_{\eta\eta} + F_\eta^2 F_{\xi\xi} + 4F_\xi F_\eta F_{\xi\eta}). \end{aligned} \tag{3.12}$$

There is two-fold symmetry in the ξ–η plane; there are two perpendicular symmetry

axes, but they are not equivalent. The ξ direction lies along one symmetry axis, which is also one of the crystalline axes, and the η direction lies along the other symmetry axis, as shown in figure 1*c*.

The marginal stability condition for growth in the [011] direction is found by maximizing μ^{-1} over the neutral surface:

$$\mu^{-1} = a^2 \left[1 - \frac{2\nu\tilde{\gamma}_2}{1-\nu}\sin^2\chi\right] - \frac{1}{4}(1-\nu^2)a^4, \tag{3.13}$$

where the wavevector of the perturbation is $(a\cos\chi, a\sin\chi)$. The global maximum is at

$$\cos\chi = 0, \quad a^2 = 2[1 - 2\nu\tilde{\gamma}_2/(1-\nu)]/(1-\nu^2), \tag{3.14}$$

if $\tilde{\gamma}_2 < 0$ ($\gamma_2 < 1$), and at

$$\sin\chi = 0, \quad a^2 = 2/(1-\nu^2) \tag{3.15}$$

otherwise. So η-rolls become unstable first if $\gamma_2 < 1$, and ξ-rolls if $\gamma_2 > 1$.

Linear selection is dominant for growth in the [011] direction, and rolls are preferred. The competition between rolls and more complex patterns such as rectangles or hexagons, can be studied if $\tilde{\gamma}_2$ is small (equivalently γ_2 is close to 1), so that the marginal stability condition is given by (3.9) to leading order, with $a = a_c$ and $\mu^{-1} = \mu_c^{-1}$ as defined in equations (3.10) and (3.11) above. In all that follows, we shall drop the subscript from the critical wavenumber and understand that from now on $a \equiv a_c$.

The above generalized Brattkus–Davis equations serve as the starting point for our study of pattern-forming bifurcations in the presence of anisotropy.

4. Equations governing rectangle/roll and hexagon/roll competition: effects of anisotropy

To investigate rectangle/roll competition, consider small amplitude solutions of the form

$$F = \delta\{A(T)e^{ia(\xi\cos\psi+\eta\sin\psi)} + B(T)e^{ia[\xi\cos(\psi+\theta)+\eta\sin(\psi+\theta)]} + \text{c.c.}\} + \text{h.o.t.}, \tag{4.1}$$

where here and hereafter, c.c. denotes complex conjugate and h.o.t. stands for higher order terms, and where $0 < \delta \ll 1$ is a small parameter which measures the distance from threshold:

$$\mu^{-1} = \mu_c^{-1} - s\delta^2. \tag{4.2}$$

Here s measures the degree of sub- or supercriticality. The time is rescaled so that $\partial_\tau = \delta^2\partial_T$. Here A is the amplitude of rolls whose axes are aligned at an angle ψ to the η axis, and B is the amplitude of rolls whose axes are aligned at an angle $\psi + \theta$ to the η axis. The angular separation of the two rolls is therefore θ, as shown in figure 2*a*. A superposition of the two sets of rolls results in a square ($\theta = \pi/2$) or rectangular pattern, as illustrated in figure 3. We must have $\theta \neq \pm 2\pi/3$, or else a hexagonal pattern will be favoured through resonant-triad interactions. A weakly nonlinear analysis of the modified Brattkus–Davis equation results in a pair of coupled equations for the evolution of the amplitudes. In the most general case allowed by the expansion (2.7) of I, they take the form

$$a^2\frac{dA}{dT} = (s - s_1)A - (\alpha_1|A|^2 + \alpha_2|B|^2)A, \tag{4.3a}$$

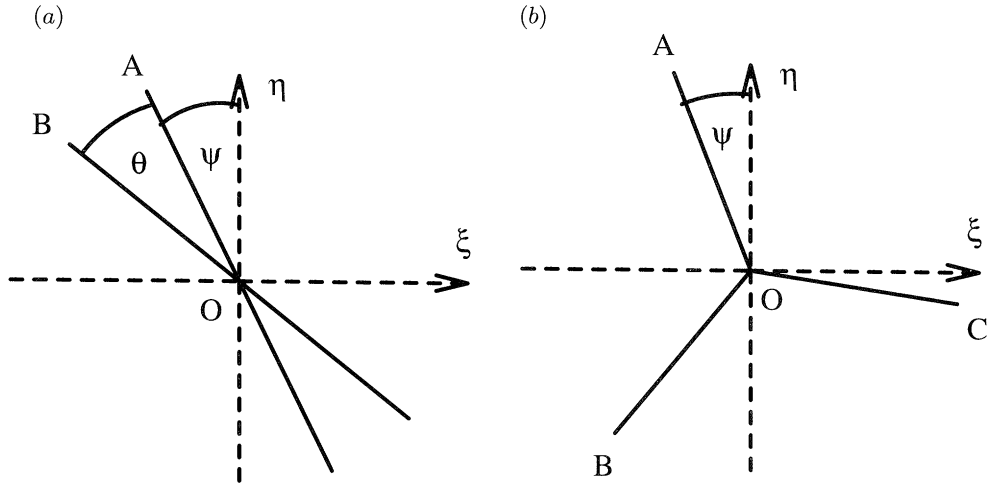

Figure 2. In roll/rectangle competition, the axes of the A-rolls lie at an angle ψ to the η axis, and the axes of the B-rolls at an angle $\psi+\theta$. The two sets of rolls are separated by an angle θ. (b) In roll/hexagon competition, the axes of the A-rolls lie at an angle ψ to the η axis, the axes of the B-rolls at an angle $\psi+2\pi/3$ and the axes of the C-rolls at an angle $\psi-2\pi/3$. Each set of rolls is separated from its neighbours by an angle of $2\pi/3$. The relationship of the η direction to the crystalline axes for growth in the [100], [011] and [111] directions is summarized in figure 1.

$$a^2\frac{\mathrm{d}B}{\mathrm{d}T} = (s-s_2)B - (\beta_1|B|^2+\beta_2|A|^2)B, \tag{4.3\,b}$$

where s_1 and s_2 are real, and the α_i and β_j are complex. Although the environment is anisotropic, the real parts of the coupling coefficients preserve chiral symmetry, so that $\mathrm{Re}(\alpha_2)=\mathrm{Re}(\beta_2)$. The exact form of the coefficients s_i, α_j, and β_k is found for each growth direction from the analysis of the appropriate long-wave evolution equation (Hoyle *et al.* 1995). In the isotropic case, all the coefficients are real, and certain additional relationships between the coefficients hold. In particular, we find that $s_1=s_2=0$, say, and $\alpha_1=\beta_1$, along with $\alpha_2=\beta_2$. Figure 4 shows a typical bifurcation diagram for the isotropic case. Some of the possible bifurcation diagrams for the case of anisotropy with real coefficients are given in Golubitsky & Schaeffer (1985).

To investigate hexagon/roll competition, consider small amplitude solutions of the form

$$\begin{aligned} F = \delta\{&A(T)\mathrm{e}^{\mathrm{i}a(\xi\cos\psi+\eta\sin\psi)} + B(T)\mathrm{e}^{\mathrm{i}a\{\xi\cos(\psi+2\pi/3)+\eta\sin(\psi+2\pi/3)\}} \\ &+C(T)\mathrm{e}^{\mathrm{i}a\{\xi\cos(\psi-2\pi/3)+\eta\sin(\psi-2\pi/3)\}} + \mathrm{c.c.}\} + \mathrm{h.o.t.}, \end{aligned} \tag{4.4}$$

where A is the amplitude of rolls whose axes are aligned at an angle ψ to the η axis, while the B rolls lie at an angle $2\pi/3$ to the A rolls, and the C rolls are at an angle $2\pi/3$ to the B rolls, as illustrated in figure 2b. The evolution takes place on a perfect hexagonal lattice. An equal superposition of all three sets of rolls results in a hexagonal pattern, illustrated in figure 10a. A weakly nonlinear analysis of the modified Brattkus–Davis equation results in a set of coupled amplitude equations. The most general form allowed by the expansion (2.7) of I, is given by

$$a^2\frac{\mathrm{d}A}{\mathrm{d}T} = (s-s_1)A + \alpha\bar{B}\bar{C} - (\nu_1|A|^2+\nu_2|B|^2+\nu_3|C|^2)A, \tag{4.5\,a}$$

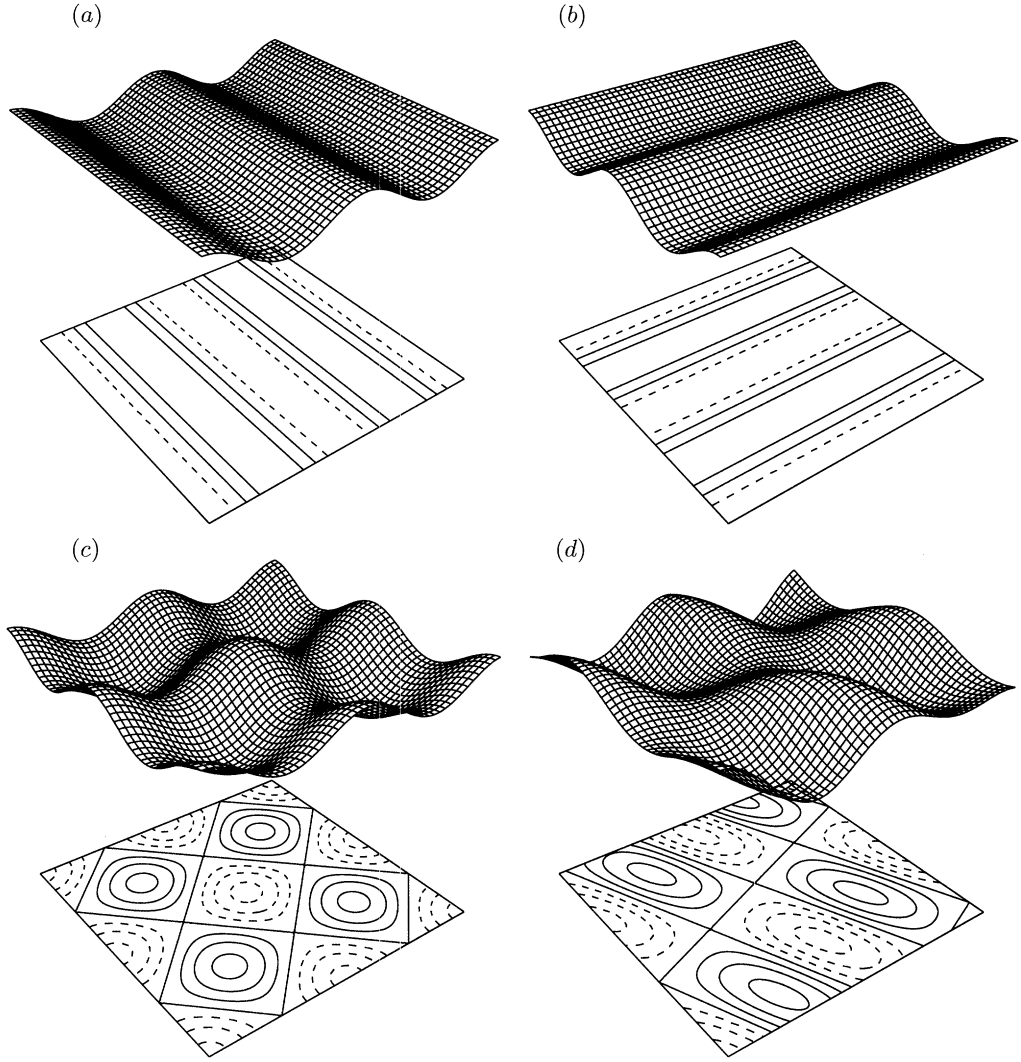

Figure 3. Examples of interface shapes for rolls in (*a*) the ξ-direction and (*b*) the η-direction, and the resulting shape for a superposition of two rolls producing (*c*) a square pattern or (*d*) a rectangular pattern. The diagrams show a surface plot of the scaled interface position, $F = \delta\{A(T)\mathrm{e}^{\mathrm{i}a(\xi\cos\psi+\eta\sin\psi)} + B(T)\mathrm{e}^{\mathrm{i}a\{\xi\cos(\psi+\theta)+\eta\sin(\psi+\theta)\}} + \text{c.c.}\}$, with a contour plot projected onto a horizontal plane below.

$$a^2\frac{\mathrm{d}B}{\mathrm{d}T} = (s-s_2)B + \alpha\bar{C}\bar{A} - (\nu_4|B|^2 + \nu_5|C|^2 + \nu_2|A|^2)B, \tag{4.5\,b}$$

$$a^2\frac{\mathrm{d}C}{\mathrm{d}T} = (s-s_3)C + \alpha\bar{A}\bar{B} - (\nu_6|C|^2 + \nu_3|A|^2 + \nu_5|B|^2)C, \tag{4.5\,c}$$

where the s_i and the ν_j are real, α is complex, and the overbar denotes complex conjugate. These equations preserve chiral symmetry. Again the exact form of the coefficients is found from the modified Brattkus–Davis equation (Hoyle *et al.* 1995). If the coefficients of the quadratic terms in the amplitude equations are of size $O(\delta^0)$, then time must be rescaled so that $\partial_\tau = \delta\partial_T$, and the amplitude equations must be truncated at quadratic order. However, if the quadratic terms are of size $O(\delta)$, time

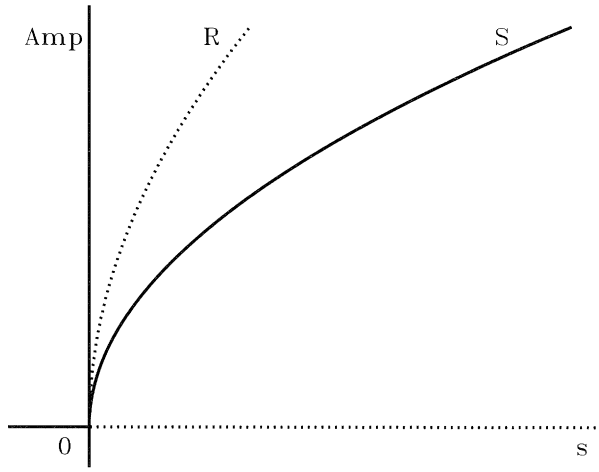

Figure 4. Typical bifurcation diagram for squares in the isotropic case, with $\alpha_2 > \alpha_1 > 0$. Dotted lines indicate an unstable solution, and solid lines a stable one. The dotted curve, labelled R, shows the amplitude of A or B rolls, and the solid curve, labelled S, the amplitude of rectangles.

is rescaled so that $\partial_\tau = \delta^2 \partial_T$, and cubic order terms in the amplitude equations are retained. In the isotropic case, there are additional relationships among the coefficients. In particular, we find that $s_1 = s_2 = s_3 = 0$, say, $\nu_1 = \nu_4 = \nu_6$ and $\nu_2 = \nu_3 = \nu_5$, and that all the coefficients are real. When anisotropy is present, we retain the perfect hexagonal lattice upon which the pattern evolution takes place, but the symmetry revealed in these relationships between the coefficients is lost. Figure 5 shows the bifurcation diagram for the isotropic case, in the parameter regime $\alpha > 0$, $0 < \nu_1 < \nu_2$; it is equivalent to the bifurcation diagram given by Busse (1967) if the mixed mode is omitted.

In the following sections we shall consider the existence and stability of solutions to the amplitude equations (4.3 *a*) and (4.3 *b*), and (4.5 *a*), (4.5 *b*) and (4.5 *c*) in the special cases of growth in the [100], [111] and [011] directions. The amplitude equations are derived here in the context of directional solidification. However, equations (4.3 *a*), (4.3 *b*) are quite general, while equations (4.5 *a*)–(4.5 *c*) hold for a wide class of anisotropies, so both sets are applicable to anisotropic pattern formation in more general physical systems. A solid with anisotropies in the kinetic coefficient or in thermal conductivity would be expected to lie in this class. For another example, liquid nematic crystals have an orientational ordering characterized by a director $\boldsymbol{n}$; this anisotropy affects pattern formation during electrohydrodynamic convection (Kai & Hirakawa 1978; Joets & Ribotta 1988).

5. Growth in the [100] direction: anisotropy delayed to cubic order

When the growth direction is [100], the effect of anisotropy first appears in the coefficients of the cubic terms in the amplitude equations. Linear pattern selection is unaffected, and quadratic terms also remain unaltered.

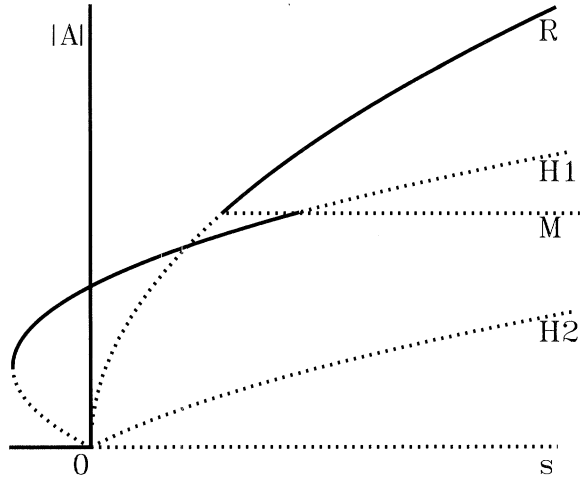

Figure 5. Schematic bifurcation diagram for hexagons in the isotropic case. The amplitude $|A|$ is plotted against s for the roll-solution branch (labelled R) with $|B| = |C| = 0$, for the mixed-mode branch (labelled M) with $|A|$ constant and $|B| = |C|$, and for the two hexagon-solution branches with $|A| = |B| = |C|$. Here unstable solution branches are indicated by dotted curves, and stable branches by solid curves. The curves labelled H1 and H2 correspond to the solutions with $|A| = |B| = |C|$, with $\Phi_S = 0$ and $\Phi_S = \pi$, respectively. Branches where all three components of the solution are stable are indicated by solid curves, and branches where one or more components are unstable are indicated by dotted curves. Consequently, the behaviour of three growth rate eigenvalues is projected onto the bifurcation diagram for one component, and in this way our representation differs from the usual one.

(*a*) *Roll/rectangle competition*

Roll/rectangle competition for growth in the [100] direction is governed by the equations

$$a^2 \frac{\mathrm{d}A}{\mathrm{d}T} = sA - (\alpha_1|A|^2 + \alpha_2|B|^2)A, \tag{5.1a}$$

$$a^2 \frac{\mathrm{d}B}{\mathrm{d}T} = sB - (\beta_1|B|^2 + \beta_2|A|^2)B, \tag{5.1b}$$

where

$$\alpha_1 = \frac{8a^6}{9} + 12a^4\gamma_4 + 3a^4(\gamma_5 - 2\gamma_4)\sin^2 2\psi, \tag{5.2a}$$

$$\beta_1 = \frac{8a^6}{9} + 12a^4\gamma_4 + 3a^4(\gamma_5 - 2\gamma_4)\sin^2 2(\psi + \theta), \tag{5.2b}$$

$$\begin{aligned}\alpha_2 = \beta_2 = {} & \frac{8a^6}{(1 - 4\cos^2\theta)^2}[\nu(1 - 2\nu) - (2 - 5\nu + 4\nu^2)\cos^2\theta \\ & +2(2 - 7\nu + 7\nu^2)\cos^4\theta + 8\nu(1 - \nu)\cos^6\theta] \\ & +8a^4\gamma_4(1 + 2\cos^2\theta) + 4a^4(\gamma_5 - 2\gamma_4)\sin^2\theta \\ & +3a^4(\gamma_5 - 2\gamma_4)[\cos 2\theta - \cos(4\psi + 2\theta)].\end{aligned} \tag{5.2c}$$

In the isotropic case, we have $\gamma_5 = 2\gamma_4 = -\frac{1}{4}$ (McFadden *et al.* 1988). The effect of anisotropy on the coefficients is shown in the parts proportional to γ_4 and to $\gamma_5 - 2\gamma_4$, which appear only in the cubic terms. Note that all the coefficients remain real, and

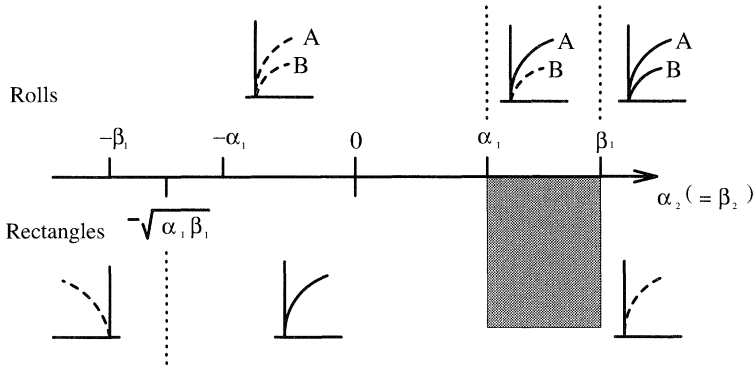

Figure 6. Schematic diagram showing changes in bifurcation structure with varying α_2; here $0 < \alpha_1 < \beta_1$. Insets shown above the α_2-axis correspond to the two branches of roll solutions, and insets below the axis correspond to the rectangular-solution branches. There are no rectangle solutions in the shaded region.

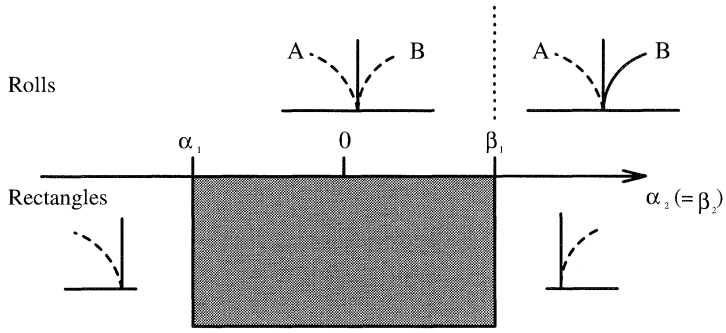

Figure 7. Schematic diagram showing changes in bifurcation structure with varying α_2; here $\alpha_1 < 0 < \beta_1$. Insets shown above the α_2-axis correspond to the two branches of roll solutions, and insets below the axis correspond to the rectangular solution branches. There are no rectangle solutions in the shaded region.

the coefficients of the linear terms are equal, just as in the isotropic case; only the cubic coefficients are affected by the anisotropy.

(i) *Overview of stability conditions*

The possible steady solutions are the trivial solution $A = B = 0$, A rolls at an angle ψ to the η axis, $A \neq 0$ and $B = 0$, B rolls at an angle $\psi + \theta$ to the η axis, $A = 0$ and $B \neq 0$, and rectangles, $A \neq 0$ and $B \neq 0$.

The stability results are summarized in figures 6, 7 and 8. For fixed values of α_1 and β_1, the figures show how the bifurcation structure changes as α_2 ranges over various intervals. The region above the α_2-axis depicts the situation for the two roll solutions, and the region below the axis is devoted to the rectangular solutions. In the schematic bifurcation diagrams, stable (unstable) solutions are indicated by solid (dashed) curves. In the isotropic case, we have $\alpha_1 = \beta_1 > 0$; see figure 6. The position on the α_2 axis would depend on the value of θ. For $\alpha_2 < -\alpha_1$, rolls are supercritical and unstable, while rectangles are subcritical and unstable. For $-\alpha_1 < \alpha_2 < \alpha_1$, rolls

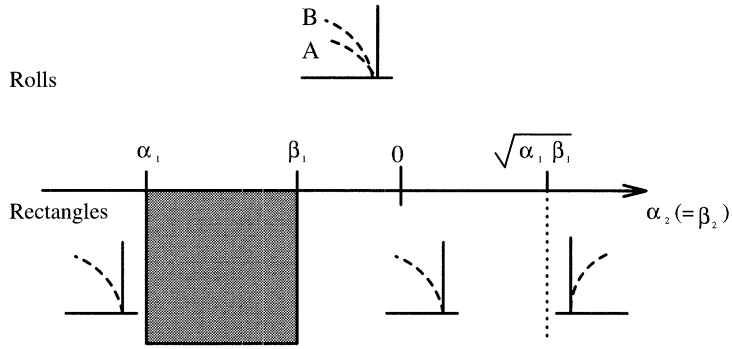

Figure 8. Schematic diagram showing changes in bifurcation structure with varying α_2; here $\alpha_1 < \beta_1 < 0$. Insets shown above the α_2-axis correspond to the two branches of roll solutions, and insets below the axis correspond to the rectangular solution branches. There are no rectangle solutions in the shaded region.

are still unstable and supercritical, but rectangles are now stable and supercritical. Finally, if $\alpha_2 > \alpha_1$, rolls are stable and supercritical, while rectangles are unstable and supercritical. When anisotropy is introduced, we find that α_1 and β_1 are no longer equal in value. For weak anisotropy, we have the situation depicted in figure 6, where $\beta_1 > \alpha_1 > 0$ (or similarly $\alpha_1 > \beta_1 > 0$). This situation may persist for stronger anisotropies. Alternatively, for large negative values of $\gamma_5 - 2\gamma_4$, one (figure 7) or both (figure 8) of α_1 and β_1 may become negative, depending on the values of ψ and θ.

Figure 6 summarizes the results for the case $\beta_1 > \alpha_1 > 0$, where the roll solutions both bifurcate supercritically. For the roll solutions, the amplitude of the roll solution branch with $R_A \neq 0$ (labelled 'A' in the insets) is larger than the amplitude of the roll solution branch with $R_B \neq 0$ (labelled 'B'). For $\alpha_2 > \beta_1$, both roll branches are stable. For $\alpha_1 < \alpha_2 < \beta_1$, the A-roll is stable and the B-roll is unstable. For $\alpha_2 < \alpha_1$, both rolls are unstable. For the rectangular-solution branch, represented by the diagrams below the axis, the branch is supercritical but unstable for $\alpha_2 > \beta_1$. The shaded area represents the interval $\alpha_1 < \alpha_2 < \beta_1$ where no rectangular solutions exist. For $-\sqrt{\alpha_1\beta_1} < \alpha_2 < \alpha_1$, the branch is supercritical and stable. For $\alpha_2 < -\sqrt{\alpha_1\beta_1}$ the branch is subcritical and unstable. In the case $\alpha_1 > \beta_1 > 0$, this summary would apply if α_1 and β_1, and A and B were interchanged throughout.

Figure 7 summarizes the stability results for the case $\alpha_1 < 0 < \beta_1$ in a similar fashion. The A-roll is subcritical and unstable; the B-roll is stable for $\alpha_2 > \beta_1$ and is unstable for $\alpha_2 < \beta_1$. The rectangular solution branch is never stable; it is supercritical for $\alpha_2 > \beta_1$, does not exist for $\alpha_1 < \alpha_2 < \beta_1$, and is subcritical for $\alpha_2 < \alpha_1$. Again, this summary is applicable to the case $\beta_1 < 0 < \alpha_1$, if α_1 and β_1, and A and B are interchanged throughout.

Figure 8 gives the linear stability results when $\alpha_1 < \beta_1 < 0$. Both A-rolls and B-rolls are subcritical and unstable. The rectangular solution branch is never stable; it is supercritical for $\alpha_2 > \sqrt{\alpha_1\beta_1}$, subcritical for $\beta_1 < \alpha_2 < \sqrt{\alpha_1\beta_1}$, does not exist for $\alpha_1 < \alpha_2 < \beta_1$, and is subcritical for $\alpha_2 < \alpha_1$. This summary applies to the case $\beta_1 < \alpha_1 < 0$, if α_1 and β_1, and A and B are interchanged throughout.

(ii) *Existence and stability requirements for rolls and rectangles*

The possible steady solutions are the trivial solution $A = B = 0$, A rolls at an angle ψ to the η axis

$$|A|^2 = s/\alpha_1 > 0, \quad B = 0, \tag{5.3}$$

B rolls whose axes are aligned at an angle $(\psi + \theta)$ to the η axis

$$A = 0, \quad |B|^2 = s/\beta_1 > 0, \tag{5.4}$$

and rectangles

$$|A|^2 = \frac{s(\beta_1 - \alpha_2)}{(\alpha_1\beta_1 - \alpha_2^2)} > 0, \quad |B|^2 = \frac{s(\alpha_1 - \alpha_2)}{(\alpha_1\beta_1 - \alpha_2^2)} > 0. \tag{5.5}$$

Rectangles do not exist in the case $\min(\alpha_1, \beta_1) < \alpha_2 < \max(\alpha_1, \beta_1)$.

The A rolls bifurcate supercritically if $\alpha_1 > 0$, and subcritically otherwise. Similarly, the B rolls bifurcate supercritically if $\beta_1 > 0$, and subcritically otherwise. Rectangles bifurcate supercritically if $(\beta_1 - \alpha_2)/(\alpha_1\beta_1 - \alpha_2^2) > 0$, and $(\alpha_1 - \alpha_2)/(\alpha_1\beta_1 - \alpha_2^2) > 0$, and subcritically otherwise.

The stability of these solutions to amplitude perturbations is easily determined. The trivial solution is stable when $s < 0$ and unstable when $s > 0$. A rolls are stable when $s > 0$ and $(1 - \alpha_2/\alpha_1) < 0$, and unstable otherwise. B rolls are stable for $s > 0$ and $(1 - \alpha_2/\beta_1) < 0$, and unstable otherwise. Rectangles are stable if $s(2\alpha_1\beta_1 - \alpha_1\alpha_2 - \beta_1\alpha_2)/(\alpha_1\beta_1 - \alpha_2^2) > 0$ and $(\alpha_1 - \alpha_2)(\beta_1 - \alpha_2)/(\alpha_1\beta_1 - \alpha_2^2) > 0$, and unstable otherwise. Note that for rectangles to be stable we must have $s > 0$. Together with the existence conditions for rectangles, this implies that we must have $\alpha_1 > 0$ and $\beta_1 > 0$ for stability.

In the isotropic case, $\gamma_5 = 2\gamma_4 = -\frac{1}{4}$; rolls bifurcate supercritically, since $a^2 > 2 > 27/16$. In the anisotropic case, however, rolls in certain parameter regimes may bifurcate supercritically $s > 0$, or subcritically $s < 0$, depending upon the orientation, ψ, of the roll. If $\gamma_5 - 2\gamma_4 < 0$ and $8a^2/9 + 12\gamma_4 > 0$, rolls in the vicinity of $\psi = 0$ and $\pi/2$ are supercritical, the exact range being given by

$$0 \leqslant \sin^2 2\psi < -\frac{8a^2/9 + 12\gamma_4}{3(\gamma_5 - 2\gamma_4)}. \tag{5.6}$$

At all other angles, rolls are subcritical. If $\gamma_5 - 2\gamma_4 > 0$ and $8a^2/9 + 12\gamma_4 > 0$, rolls are supercritical at all possible angles ψ. If $8a^2/9 + 12\gamma_4 < 0$ and $8a^2/9 + 6\gamma_4 + 3\gamma_5 > 0$, rolls in the vicinity of $\psi = \pi/4$ and $3\pi/4$ are supercritical, the exact range being given by

$$1 \geqslant \sin^2 2\psi > -\frac{8a^2/9 + 12\gamma_4}{3(\gamma_5 - 2\gamma_4)}. \tag{5.7}$$

Rolls at other angles are subcritical. If $8a^2/9 + 12\gamma_4 < 0$ and $8a^2/9 + 6\gamma_4 + 3\gamma_5 < 0$, rolls are subcritical at any angle ψ. The fourfold symmetry associated with the [100] direction is reflected in the orientation of sub- and supercritical rolls. This is shown in the $\sin^2 2\psi$ dependence of α_1.

To investigate the effect of anisotropy on the existence and stability of rectangles, we will consider the special case of squares, where $\theta = \pi/2$. The coupling coefficients are then given by

$$\alpha_1 = \beta_1 = 8a^6/9 + 12a^4\gamma_4 + 3a^4(\gamma_5 - 2\gamma_4)\sin^2 2\psi, \tag{5.8 a}$$

$$\alpha_2 = 8a^6\nu(1-2\nu) + 2a^4(\gamma_5 - 2\gamma_4)(2 - 3\sin^2 2\psi) + 8a^4\gamma_4. \qquad (5.8\,b)$$

Squares bifurcate supercritically if

$$3a^4(\gamma_5 - 2\gamma_4)\sin^2 2\psi < 8a^6(1/9 + \nu - 2\nu^2) + 12a^4\gamma_4 + 4a^4\gamma_5, \qquad (5.9)$$

and subcritically otherwise. Consequently, in certain parameter regimes, the direction of bifurcation will depend on the orientation, ψ, of the squares. If $8a^2(1/9 + \nu - 2\nu^2) + 12\gamma_4 + 4\gamma_5 > \max\{0, 3(\gamma_5 - 2\gamma_4)\}$, then squares at all orientations bifurcate supercritically. If $8a^2(1/9+\nu-2\nu^2)+12\gamma_4+4\gamma_5 < \min\{0, 3(\gamma_5-2\gamma_4)\}$, then squares at all orientations bifurcate subcritically. When $3(\gamma_5 - 2\gamma_4) > 8a^2(1/9 + \nu - 2\nu^2) + 12\gamma_4 + 4\gamma_5 > 0$, squares bifurcate supercritically for orientations close to $\psi = 0, \pi/2$, the exact range being given by $\sin^2 2\psi < \{8a^2(1/9+\nu-2\nu^2)+12\gamma_4+4\gamma_5\}/3(\gamma_5-2\gamma_4)$, and subcritically otherwise. When $3(\gamma_5 - 2\gamma_4) < 8a^2(1/9+\nu-2\nu^2)+12\gamma_4+4\gamma_5 < 0$, the squares bifurcate supercritically for orientations close to $\psi = \pi/4, 3\pi/4$, the exact range being given by $\sin^2 2\psi > \{8a^2(1/9+\nu-2\nu^2)+12\gamma_4+4\gamma_5\}/3(\gamma_5-2\gamma_4)$, and subcritically otherwise. This behaviour contrasts with that in the isotropic case where squares bifurcate supercritically if $-13/9 + 32\nu - 59\nu^2 > 0$, and subcritically otherwise, for all orientations ψ. In other words, in the isotropic case the value of ν is enough to determine the direction of bifurcation. When anisotropy is present, however, the bifurcation can be either sub- or supercritical at one given value of ν depending upon the orientation of the pattern.

For $s > 0$ and $\alpha_1 > 0$, rectangles are the stable preferred pattern when $-\alpha_1 < \alpha_2 < \alpha_1$, and rolls are the preferred pattern for $\alpha_2 > \alpha_1$. In the isotropic case, we have $\alpha_1 = 8a^6/9 - 3a^4/2 > 0$ and $\alpha_2 = 8a^6\nu(1-2\nu) - a^4$. Then $\alpha_1 - \alpha_2$ is positive if $(23/9 - 32\nu + 65\nu^2) > 0$, and negative otherwise, while $\alpha_1 + \alpha_2$ is positive if $-13/9 + 32\nu - 59\nu^2 > 0$ and negative otherwise. So in the approximate range $0.1 < \nu < 0.4$, we have $\alpha_2 > \alpha_1$ and roll solutions are the stable, preferred modes. Squares bifurcate supercritically in this range, but are unstable to a symmetry-breaking perturbation. (This range includes the value $\nu \sim 1/3$ that is appropriate for the roll-hexagon competition for $k \sim 1$ considered by Brattkus & Davis (1988).) For values of ν outside this range, roll solutions are unstable. Square solutions are stable immediately outside this range, where $-\alpha_1 < \alpha_2 < \alpha_1$; in these intervals, squares bifurcate supercritically and are the preferred mode. For extreme values of ν near $\nu = 0$ and $\nu = 1$, we have $\alpha_2 < -\alpha_1 < 0$, and the squares bifurcate subcritically; in these intervals there are no stable solutions of either type.

For squares in the presence of anisotropy, we find that

$$\alpha_1 - \alpha_2 = 8a^6(1/9 - \nu + 2\nu^2) + 4a^4\gamma_4 + a^4(\gamma_5 - 2\gamma_4)(9\sin^2 2\psi - 4).$$

Considering the effect of each of the two components of anisotropy γ_4 and $(\gamma_5 - 2\gamma_4)$ separately, we find that increasing γ_4 above its isotropic value of $-\frac{1}{8}$, increases $\alpha_1 - \alpha_2$ and so favours stable squares over rolls, whereas increasing $\gamma_5 - 2\gamma_4$ above its isotropic value of zero, increases $\alpha_1 - \alpha_2$ if $\sin^2 2\psi > 4/9$, thus favouring stable squares, and decreases the value of $\alpha_1 - \alpha_2$ otherwise, favouring stable rolls.

(*b*) *Roll/hexagon competition*

Roll/hexagon competition is governed by the amplitude equations,

$$a^2 A_T = sA + \alpha\bar{B}\bar{C} - [\mu_1 + \mu_3(\psi)]|A|^2 A - [\mu_2 + \mu_4(\psi)]|B|^2 A \\ -[\mu_2 + \mu_4(\psi - 2\pi/3)]|C|^2 A, \qquad (5.10\,a)$$

$$a^2 B_T = sB + \alpha \bar{C}\bar{A} - [\mu_1 + \mu_3(\psi + 2\pi/3)]|B|^2 B - [\mu_2 + \mu_4(\psi + 2\pi/3)]|C|^2 B - [\mu_2 + \mu_4(\psi)]|A|^2 B, \quad (5.10\,b)$$

$$a^2 C_T = sC + \alpha \bar{A}\bar{B} - [\mu_1 + \mu_3(\psi - 2\pi/3)]|C|^2 C - [\mu_2 + \mu_4(\psi - 2\pi/3)]|A|^2 C - [\mu_2 + \mu_4(\psi + 2\pi/3)]|B|^2 C, \quad (5.10\,c)$$

where

$$\alpha = \tfrac{1}{2}(1 - 3\nu)a^4, \quad (5.11\,a)$$

$$\mu_1 = 2(1 + 6\gamma_4)a^4, \quad (5.11\,b)$$

$$\mu_2 = (9/4 + 12\gamma_4)a^4, \quad (5.11\,c)$$

$$\mu_3(\theta) = 3a^4(\gamma_5 - 2\gamma_4)\sin^2 2\theta, \quad (5.11\,d)$$

$$\mu_4(\theta) = 2a^4(\gamma_5 - 2\gamma_4)\{2\sin^2(2\theta + 2\pi/3) + \sin 2\theta \sin(2\theta - 2\pi/3)\}. \quad (5.11\,e)$$

If $|1 - 3\nu|$ is a unit-order constant, we must truncate the amplitude equations at second order, whereas if $|1 - 3\nu|$ is small, third-order terms must be included. In calculating the coefficients of the cubic terms, it is assumed that $|1 - 3\nu|$ is indeed small, from which we also deduce that $a^2 = 9/4$. The limit $\nu \sim 1/3$ is the limit $k \to 1$ at constant M (fixed undercooling) and constant Γ (fixed surface energy), and was investigated in the isotropic case by Brattkus & Davis (1988). The anisotropy appears in the coefficients of the cubic terms. Once again, it is only the real parts of the cubic coefficients which are affected by the anisotropy; all the coefficients are real, and the linear and quadratic coefficients are unchanged from their values in the isotropic case.

Note that when the surface energy is isotropic, $2\gamma_4 = \gamma_5 = -\frac{1}{4}$, the cubic coefficients take the forms $\mu_1 = a^4/2 > 0$ and $\mu_1 - \mu_2 = -a^4/4 < 0$, so that the bifurcation structure is as depicted in figure 5. When anisotropy is introduced, we shall see that we no longer find perfect hexagons $R_A = R_B \neq 0$. Owing to the loss of symmetry, there is no longer a clear distinction between mixed modes ($R_A \neq R_B$) and hexagon-type solutions. The mixed-mode and hexagon solution branches merge into each other, and the sharp intersection between them breaks. We shall assume that the departure from isotropy is small with $|\gamma_5 + \frac{1}{4}| \ll 1$ and $|\gamma_4 + \frac{1}{8}| \ll 1$, so that the modifications to the underlying bifurcation structure of the isotropic case will also be small. In particular, we shall require $\mu_1 + \mu_3(\theta) > 0$, so that rolls bifurcate supercritically.

To understand the bifurcation structure of the amplitude equations, it is helpful to consider the special case $\psi = 0$, where the axis of one roll is aligned along one of the crystalline axes. This means that the system has twofold symmetry about the crystalline axis. Steady solutions are given by

$$A = R_A e^{i\Phi_A}, \quad B = R_B e^{i\Phi_B}, \quad C = R_C e^{i\Phi_C}, \quad (5.12)$$

with

$$0 = sR_A + \alpha R_B R_C - \mu_1 R_A^3 - \lambda_1(R_B^2 + R_C^2)R_A, \quad (5.13\,a)$$

$$0 = sR_B + \alpha R_A R_C - (\mu_1 + \lambda_2)R_B^3 - (\lambda_1 - 2\lambda_2)R_C^2 R_B - \lambda_1 R_A^2 R_B, \quad (5.13\,b)$$

$$0 = sR_C + \alpha R_A R_B - (\mu_1 + \lambda_2)R_C^3 - \lambda_1 R_A^2 R_C - (\lambda_1 - 2\lambda_2)R_B^2 R_C, \quad (5.13\,c)$$

where $\lambda_1 = \mu_2 + \mu_4(0)$ and $\lambda_2 = -9a^4(2\gamma_4 - \gamma_5)/4$. If R_A, R_B and R_C are all non-zero,

we also have

$$\sin(\Phi_A + \Phi_B + \Phi_C) = 0. \tag{5.14}$$

Consider solutions with $R_B = R_C$. These are given by

$$0 = sR_A + \alpha R_B^2 - \mu_1 R_A^3 - 2\lambda_1 R_B^2 R_A, \tag{5.15a}$$

$$0 = sR_B + \alpha R_A R_B - (\mu_1 + \lambda_1 - \lambda_2) R_B^3 - \lambda_1 R_A^2 R_B. \tag{5.15b}$$

First consider $\lambda_2 = 0$, which includes the isotropic case $2\gamma_4 = \gamma_5 = -\frac{1}{4}$. Steady hexagons are given by $R_A = R_B \neq 0$, with $s + \alpha R_A - (\mu_1 + 2\lambda_1) R_A^2 = 0$; if $\Phi_A + \Phi_B + \Phi_C = 0$, the hexagons are 'nodes', whereas if $\Phi_A + \Phi_B + \Phi_C = \pi$, they are 'cells' (Morris & Winegard 1969). There are also mixed modes ('Class V' solutions) with $R_A = -\alpha/(\mu_1 - \lambda_1)$ and $(\mu_1 + \lambda_1) R_B^2 = s - \mu_1 \alpha^2/(\mu_1 - \lambda_1)^2$. Steady rolls are given by $R_A^2 = s/\mu_1$, $R_B = 0$. The mixed mode solution branch intersects the hexagons at $s = \alpha^2(2\mu_1 + \lambda_1)/(\mu_1 - \lambda_1)^2$, and the branch of roll solutions at $s = \mu_1 \alpha^2/(\mu_1 - \lambda_1)^2$. If we plot R_A against s, the intersection of the mixed mode and hexagon solutions is sharp as shown in figure 5.

Now if anisotropy is introduced, so that $\lambda_2 \neq 0$, perfect hexagons $R_A = R_B \neq 0$ are no longer steady solutions. We have lost symmetry, and there are no nontrivial solutions with $R_A = R_B$. Consequently, *there is no longer a clear distinction between mixed modes*, which have $R_A \neq R_B$ even in the isotropic case, *and hexagon-type solutions*. It might then be expected that the mixed mode and hexagons merge into each other, and that the sharp intersection between them breaks. This is indeed what happens, as shown in figure 9. The control parameter s and the amplitude R_A are related by

$$s = \frac{\{[\mu_1(\mu_1 + \lambda_1 - \lambda_2) - 2\lambda_1^2] R_A^2 + 3\lambda_1 \alpha R_A - \alpha^2\} R_A}{[\alpha + (\mu_1 - \lambda_1 - \lambda_2) R_A]}. \tag{5.16}$$

The manner in which the intersection of the hexagon and mixed modes splits depends on the sign of λ_2. Figure 9 illustrates the effect of varying λ_2; the bifurcation diagrams for the cases (*a*) $\lambda_2 = 0$, (*b*) $\lambda_2 < 0$ and (*c*) $\lambda_2 > 0$ are shown. With $\lambda_2 = 0$, the bifurcation structure is identical to that in the isotropic case. Rolls, mixed modes, nodes and cells all exist, and are distinct from each other. There is a bifurcation between mixed modes and hexagonal nodes. When $\lambda_2 \neq 0$, the rolls remain distinct from the other solutions, but there is no longer a clear separation between mixed modes and hexagonal nodes or cells. The bifurcation between mixed modes and hexagonal nodes has been replaced by a merging of the mixed mode and hexagonal node solution branches. For $\lambda_2 < 0$, the left-hand mixed mode merges with the left-hand node, and the right-hand mixed mode with the right-hand node, whereas for $\lambda_2 > 0$, the left-hand mixed mode merges with the right-hand node and vice versa. In other words, the bifurcation is now imperfect. In all three cases, the mixed-mode solution bifurcates from the roll solution at $s = \mu_1 \alpha^2/(\mu_1 - \lambda_1)^2$.

If we allow ψ to be non-zero, the analysis is much more complex, although for $|\psi| \ll 1$, there are some interesting results. To first order in ψ, we find that the cubic coefficients μ_3 and μ_4 are given by

$$\mu_3(\psi) = 0, \tag{5.17a}$$

$$\mu_3(\psi + 2\pi/3) = 3a^4(\gamma_5 - 2\gamma_4)(3/4 + \sqrt{3}\psi), \tag{5.17b}$$

$$\mu_3(\psi - 2\pi/3) = 3a^4(\gamma_5 - 2\gamma_4)(3/4 - \sqrt{3}\psi), \tag{5.17c}$$

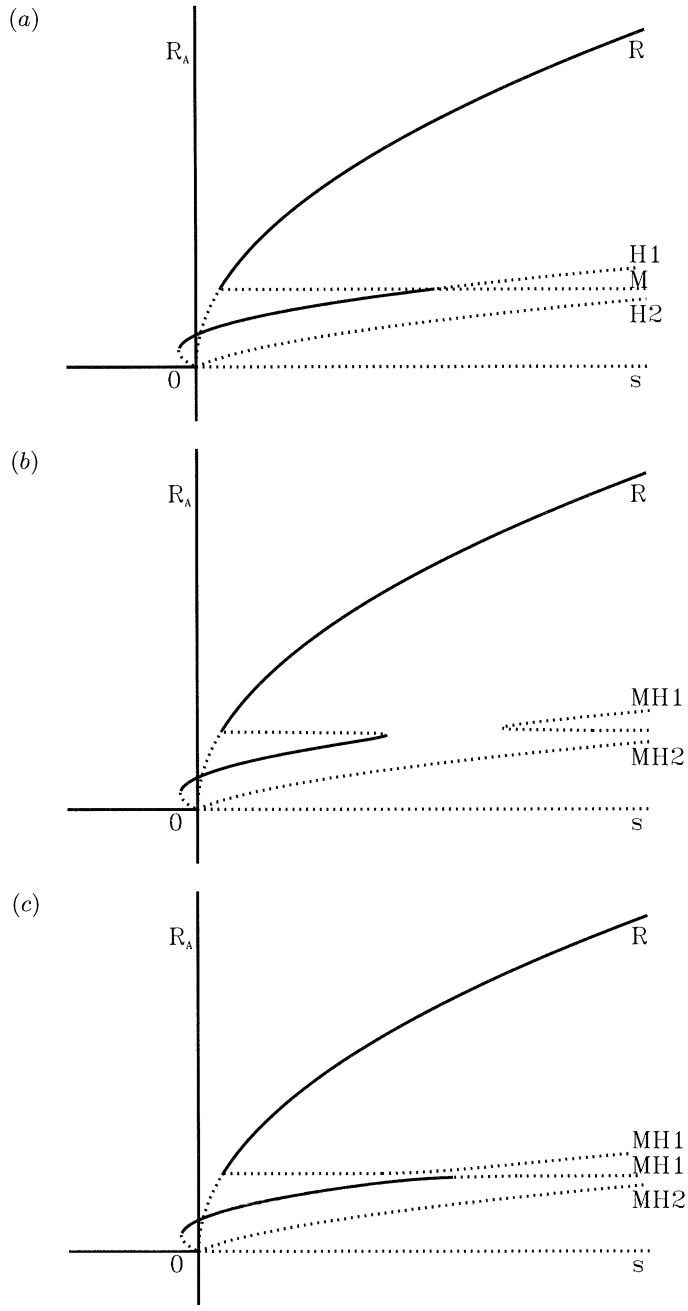

Figure 9. Bifurcation diagrams for imperfect hexagons in the [100] case, with (*a*) $\lambda_2 = 0$, (*b*) $\lambda_2 < 0$, (*c*) $\lambda_2 > 0$. The amplitude R_A is plotted against s. For $\lambda = 0$, the branches are labelled as in figure 5. When $\lambda \neq 0$, the roll-solution branch with $R_B = R_C = 0$ is labelled R, and the two combined mixed-mode and hexagon branches with $0 \neq R_A \neq R_B = R_C \neq 0$ are labelled MH1 and MH2. The curves labelled MH1 and MH2 correspond to solutions with $\Phi_S = 0$ and $\Phi_S = \pi$, respectively. Branches where all three components of the solution are stable are indicated by solid curves, and branches where one or more components are unstable are indicated by dotted curves. Consequently, the behaviour of three growth rate eigenvalues is projected onto the bifurcation diagram for one component, and in this way our representation differs from the usual one.

PHILOSOPHICAL TRANSACTIONS OF THE ROYAL SOCIETY A MATHEMATICAL, PHYSICAL & ENGINEERING SCIENCES

$$\mu_4(\psi) = 3a^4(\gamma_5 - 2\gamma_4)(1 - 2\sqrt{3}\psi), \tag{5.17 d}$$

$$\mu_4(\psi + 2\pi/3) = -3a^4(\gamma_5 - 2\gamma_4)/2, \tag{5.17 e}$$

$$\mu_4(\psi - 2\pi/3) = 3a^4(\gamma_5 - 2\gamma_4)(1 + 2\sqrt{3}\psi). \tag{5.17 f}$$

The steady solution to the amplitude equations for small ψ is expected to differ only slightly from the solution in the case $\psi = 0$. Consequently, we write

$$A = R_A(1 + r)e^{i\Phi_A}, \quad B = R_B(1 + b)e^{i\Phi_B}, \quad C = R_B(1 + c)e^{i\Phi_C}, \tag{5.18}$$

where R_A and R_B are the steady solutions for the $\psi = 0$ case, as discussed above, $|r|$, $|b|$, $|c| \ll 1$, and where

$$\sin(\Phi_A + \Phi_B + \Phi_C) = 0. \tag{5.19}$$

Substituting these expressions into the amplitude equations, we find that

$$r = O(\psi^2), \quad b = -c = \frac{3\sqrt{3}a^4(\gamma_5 - 2\gamma_4)\psi(2R_A^2 - R_B^2)}{2[\alpha R_A + (\mu_1 - \lambda_1 + 3\lambda_2)R_B^2]}. \tag{5.20}$$

So as ψ increases slightly from zero, the B and C roll amplitudes split away from each other symmetrically, while the A roll amplitude remains constant. The imperfect bifurcation structure discussed above for the $\psi = 0$ case remains embedded in the more general case of small ψ.

6. Growth in the [111] direction: anisotropy delayed to quadratic order

For solidification in the [111] direction, anisotropy does not affect linear pattern selection, but does alter the coefficients of both the quadratic and cubic terms in the amplitude equations.

(*a*) *Roll/rectangle competition*

Roll/rectangle competition for growth in the [111] direction is governed by the equations

$$a^2 A_T = sA - (\alpha_{1r} + i\alpha_{1i})|A|^2 A - (\alpha_{2r} + i\alpha_{2i})|B|^2 A, \tag{6.1 a}$$

$$a^2 B_T = sB - (\beta_{1r} + i\beta_{1i})|B|^2 B - (\beta_{2r} + i\beta_{2i})|A|^2 B, \tag{6.1 b}$$

where

$$\alpha_{1r} = \tfrac{8}{9}a^6 - \tfrac{3}{2}a^4 - \tfrac{4}{9}a^4\hat{\gamma}_3^2\cos^2 3\psi, \tag{6.2 a}$$

$$\alpha_{1i} = \tfrac{4}{3}a^5\hat{\gamma}_3\cos 3\psi, \tag{6.2 b}$$

$$\beta_{1r} = \tfrac{8}{9}a^6 - \tfrac{3}{2}a^4 - \tfrac{4}{9}a^4\hat{\gamma}_3^2\cos^2(3\psi + 3\theta), \tag{6.2 c}$$

$$\beta_{1i} = \tfrac{4}{3}a^5\hat{\gamma}_3\cos(3\psi + 3\theta), \tag{6.2 d}$$

$$\begin{aligned}\alpha_{2r} = \beta_{2r} = {} & -a^4(3\cos^2\theta + \sin^2\theta) \\ & + \frac{8a^6}{(1 - 4\cos^2\theta)^2}\{\nu(1 - 2\nu) - (2 - 5\nu + 4\nu^2)\cos^2\theta \\ & \qquad + 2(2 - 7\nu + 7\nu^2)\cos^4\theta + 8\nu(1 - \nu)\cos^6\theta\} \\ & - \frac{4a^4\hat{\gamma}_3^2}{(1 - 4\cos^2\theta)^2}\{[\cos^2(3\psi + 2\theta) + \cos^2(3\psi + \theta)](1 + 4\cos^2\theta) \\ & \qquad - 8\cos\theta\cos(3\psi + 2\theta)\cos(3\psi + \theta)\},\end{aligned} \tag{6.2 e}$$

$$\alpha_{2i} = -\frac{4a^5\hat{\gamma}_3}{(1-4\cos^2\theta)}\{\cos(3\psi+2\theta)\cos 2\theta + \cos(3\psi+\theta)\cos\theta\}, \qquad (6.2\,f)$$

$$\beta_{2i} = -\frac{4a^5\hat{\gamma}_3}{(1-4\cos^2\theta)}\{\cos(3\psi+2\theta)\cos\theta + \cos(3\psi+\theta)\cos 2\theta\}. \qquad (6.2\,g)$$

The coefficients of the linear terms are unchanged from their values in the isotropic case, and both remain real. The effect of anisotropy is shown in the coefficients of the cubic terms, which now have imaginary parts proportional to $\hat{\gamma}_3$, whereas in the isotropic case, they were purely real. There are also changes to the real parts, proportional to $\hat{\gamma}_3^2$.

If the solutions are written in polar form by setting

$$A(T) = R_A(T)\mathrm{e}^{\mathrm{i}\Phi_A(t)}, \qquad B(T) = R_B(T)\mathrm{e}^{\mathrm{i}\Phi_B(t)}, \qquad (6.3)$$

then the resulting equations have the form

$$a^2\frac{\mathrm{d}R_A}{\mathrm{d}T} = sR_A - (\alpha_{1r}R_A^2 + \alpha_{2r}R_B^2)R_A, \qquad (6.4\,a)$$

$$a^2\frac{\mathrm{d}R_B}{\mathrm{d}T} = sR_B - (\beta_{1r}R_B^2 + \beta_{2r}R_A^2)R_B, \qquad (6.4\,b)$$

$$a^2\frac{\mathrm{d}\Phi_A}{\mathrm{d}T} = -\alpha_{1i}R_A^2 - \alpha_{2i}R_B^2, \qquad (6.4\,c)$$

$$a^2\frac{\mathrm{d}\Phi_B}{\mathrm{d}T} = -\beta_{1i}R_B^2 - \beta_{2i}R_A^2. \qquad (6.4\,d)$$

The amplitudes and phases of the solutions decouple, and stability is determined by the evolution of the amplitudes. As in the [100] case, there are A-roll, B-roll and rectangular solutions. The phases Φ_A and Φ_B may evolve in time, leading to travelling wave solutions, but the phase evolution does not affect the stability characteristics. In fact, the general stability results summarized in § 5 *a* (i) and explained further in § 5 *a* (ii) hold if α_1, α_2 and β_1 are replaced by α_{1r}, α_{2r} and β_{1r} respectively.

(i) *Overview of stability conditions*

For $\hat{\gamma}_3 = 0$, the system is isotropic. As in the case of [100] growth described above, the effect of surface-tension anisotropy can be deduced by considering the dependence of α_{1r} and α_{2r} on the anisotropy coefficients. Both α_{1r} and α_{2r} depend on ${\hat{\gamma}_3}^2$; with no anisotropy, the schematic diagram shown in figure 6 degenerates into a version appropriate to the case $\alpha_{1r} = \beta_{1r} > 0$, and the stability results for the isotropic case can be recovered from these figures in that limit.

The effect of anisotropy with $\hat{\gamma}_3 \neq 0$ is to modify the real parts of the coefficients α_1 and β_1 so that they are less than $\alpha_0 \equiv 8a^6/9 - 3a^4/2$, the value in the isotropic case. In the isotropic case each set of rolls bifurcates supercritically, since $\alpha_0 > 0$. In principle, for large enough anisotropy one or both of the coefficients α_{1r} and β_{1r} can become negative, so that both sets of rolls are subcritical, or one set is subcritical while the other set is supercritical. The stability results for these cases are summarized in figures 7 and 8, if α_1, α_2 and β_1 are replaced by α_{1r}, α_{2r} and β_{1r} respectively.

(ii) *Existence and stability requirements for rolls and rectangles*

The system admits A rolls with

$$R_A^2 = s/\alpha_{1r}, \qquad R_B = 0; \tag{6.5}$$

they are stationary if $\cos 3\psi = 0$, and travelling otherwise. Similarly, B rolls

$$R_A = 0, \qquad R_B^2 = s/\beta_{1r}, \tag{6.6}$$

are stationary if $\cos(3\psi + 3\theta) = 0$, and travelling otherwise. The phase velocity is proportional to $\hat{\gamma_3}$, and to the *square* of the amplitude of the interface deformation. As for the [100] direction, A rolls are stable when $s > 0$, $(1 - \alpha_{2r}/\alpha_{1r}) < 0$, and B rolls are stable for $s > 0$, $(1 - \alpha_{2r}/\beta_{1r}) < 0$.

There are also rectangular solutions

$$R_0^2 = s(\alpha_{2r} - \beta_{1r})/(\alpha_{2r}^2 - \alpha_{1r}\beta_{1r}), \tag{6.7a}$$

$$S_0^2 = s(\alpha_{2r} - \alpha_{1r})/(\alpha_{2r}^2 - \alpha_{1r}\beta_{1r}), \tag{6.7b}$$

where $(\alpha_{2r}^2 - \alpha_{1r}\beta_{1r})$ is assumed to be non-zero. They are stationary if

$$0 = \alpha_{1i}R_0^2 + \alpha_{2i}S_0^2, \tag{6.8a}$$

$$0 = \beta_{1i}S_0^2 + \beta_{2i}R_0^2, \tag{6.8b}$$

and travelling otherwise. The phase velocity is proportional to $\hat{\gamma_3}$, and also depends on the squares of the amplitudes R_A and R_B. As for the [100] case, rectangles do not exist in the case $\min(\alpha_{1r}, \beta_{1r}) < \alpha_{2r} < \max(\alpha_{1r}, \beta_{1r})$, and are stable if

$$\frac{s(2\alpha_{1r}\beta_{1r} - \alpha_{1r}\alpha_{2r} - \beta_{1r}\alpha_{2r})}{(\alpha_{1r}\beta_{1r} - \alpha_{2r}^2)} > 0 \quad \text{and} \quad \frac{(\alpha_{1r} - \alpha_{2r})(\beta_{1r} - \alpha_{2r})}{(\alpha_{1r}\beta_{1r} - \alpha_{2r}^2)} > 0.$$

The rectangles bifurcate supercritically if $(\beta_{1r} - \alpha_{2r})/(\alpha_{1r}\beta_{1r} - \alpha_{2r}^2) > 0$, and hence also $(\alpha_{1r} - \alpha_{2r})/(\alpha_{1r}\beta_{1r} - \alpha_{2r}^2) > 0$, and subcritically otherwise.

To illustrate the effects of anisotropy, consider the specific example of squares ($\theta = \pi/2$) at an arbitrary angle ψ to the crystalline axis. The coefficients of the cubic terms take the form

$$\alpha_{1r} = \tfrac{8}{9}a^6 - \tfrac{3}{2}a^4 - \tfrac{4}{9}a^4\hat{\gamma}_3^2\cos^2 3\psi, \tag{6.9a}$$

$$\alpha_{1i} = \tfrac{4}{3}a^5\hat{\gamma}_3\cos 3\psi, \tag{6.9b}$$

$$\beta_{1r} = \tfrac{8}{9}a^6 - \tfrac{3}{2}a^4 - \tfrac{4}{9}a^4\hat{\gamma}_3^2\sin^2 3\psi, \tag{6.9c}$$

$$\beta_{1i} = \tfrac{4}{3}a^5\hat{\gamma}_3\sin 3\psi, \tag{6.9d}$$

$$\alpha_{2r} = \beta_{2r} = -a^4 + 8a^6\nu(1 - 2\nu) - 4a^4\hat{\gamma}_3^2, \tag{6.9e}$$

$$\alpha_{2i} = -4a^5\hat{\gamma}_3\cos 3\psi, \tag{6.9f}$$

$$\beta_{2i} = -4a^5\hat{\gamma}_3\sin 3\psi. \tag{6.9g}$$

Using these coefficients, it easy to show that both the A and B rolls bifurcate subcritically if

$$(16a^2 - 27)/8\hat{\gamma}_3^2 < \sin^2 3\psi < 1 - (16a^2 - 27)/8\hat{\gamma}_3^2, \tag{6.10}$$

whereas both sets of rolls are supercritical if

$$1 - (16a^2 - 27)/8\hat{\gamma}_3^2 < \sin^2 3\psi < (16a^2 - 27)/8\hat{\gamma}_3^2. \tag{6.11}$$

The A rolls bifurcate subcritically while the B rolls bifurcate supercritically if

$$\sin^2 3\psi < \min\{(16a^2 - 27)/8\hat{\gamma}_3^2, 1 - (16a^2 - 27)/8\hat{\gamma}_3^2\}, \tag{6.12}$$

and the B rolls are subcritical while the A rolls are supercritical if

$$\sin^2 3\psi > \max\{(16a^2 - 27)/8\hat{\gamma}_3^2, 1 - (16a^2 - 27)/8\hat{\gamma}_3^2\}. \tag{6.13}$$

It is possible to have one set of rolls bifurcating subcritically, and the other supercritically, and yet to have rectangles existing. This occurs if $s > 0$, $\alpha_{1r}\beta_{1r} < 0$ and $\alpha_{2r} > \max(\alpha_{1r}, \beta_{1r})$, when the rectangles are supercritical, or if $s < 0$, $\alpha_{1r}\beta_{1r} < 0$ and $\alpha_{2r} < \min(\alpha_{1r}, \beta_{1r})$, when the rectangles are subcritical.

(*b*) *Roll/hexagon competition*

Roll/hexagon competition is governed by the amplitude equations,

$$a^2 A_t = sA + (\alpha_\mathrm{r} + \mathrm{i}\alpha_\mathrm{i})\bar{B}\bar{C} - \tfrac{1}{2}a^4|A|^2A - \tfrac{3}{4}a^4(|B|^2 + |C|^2)A, \tag{6.14a}$$

$$a^2 B_t = sB + (\alpha_\mathrm{r} + \mathrm{i}\alpha_\mathrm{i})\bar{C}\bar{A} - \tfrac{1}{2}a^4|B|^2B - \tfrac{3}{4}a^4(|C|^2 + |A|^2)B, \tag{6.14b}$$

$$a^2 C_t = sC + (\alpha_\mathrm{r} + \mathrm{i}\alpha_\mathrm{i})\bar{A}\bar{B} - \tfrac{1}{2}a^4|C|^2C - \tfrac{3}{4}a^4(|A|^2 + |B|^2)C, \tag{6.14c}$$

where

$$\alpha_\mathrm{r} = \tfrac{3}{2}(\tfrac{1}{3} - \nu)a^4, \tag{6.15a}$$

$$\alpha_\mathrm{i} = -\hat{\gamma}_3 a^3 \cos 3\psi. \tag{6.15b}$$

The effect of the anisotropy is seen in the coefficient of the quadratic terms, which is purely real in the isotropic case, but has an imaginary part proportional to $\hat{\gamma}_3$ when there is anisotropy. We can write the coefficient of the quadratic term in the form

$$\tfrac{3}{2}(\tfrac{1}{3} - \nu)a^4 - \mathrm{i}\hat{\gamma}_3 a^3 \cos 3\psi = \lambda \mathrm{e}^{\mathrm{i}\Psi}, \tag{6.16}$$

where $\lambda \geqslant 0$. If λ is a unit-order constant we must truncate the expansion at second order, whereas if λ is small, the third order terms must be included. Once again, the coefficients of the cubic terms shown here are appropriate for the case when λ is small.

If the amplitude equations are truncated at quadratic order, they are equivalent to those considered by McFadden *et al.* (1988), and their analysis applies. There are steady-state solutions of the form

$$A = R_A \mathrm{e}^{\mathrm{i}\Phi_A}, \quad B = R_B \mathrm{e}^{\mathrm{i}\Phi_B}, \quad C = R_C \mathrm{e}^{\mathrm{i}\Phi_C}, \tag{6.17}$$

where R_A, R_B, $R_C \geqslant 0$. We then have

$$0 = sR_A + \lambda R_B R_C \mathrm{e}^{\mathrm{i}\Phi_S}, \tag{6.18}$$

where $\Phi_S = (\Psi - [\Phi_A + \Phi_B + \Phi_C])$. Two other equations obtained by cyclically permuting the subscripts $\{A, B, C\}$ also hold. It follows that if one of R_A, R_B and R_C vanish, they all vanish; also, if they are all non-zero, then they are equal, with $R_A = R_B = R_C = R_0 \neq 0$, say. We then have

$$\sin \Phi_S = 0, \tag{6.19}$$

and

$$s = -\lambda R_0 \cos \Phi_S, \tag{6.20}$$

so that $A = 1/\lambda$, and Φ_S is an odd integer multiple of π on the supercritical branch

($s = 1$), and is an even multiple of π on the subcritical branch ($s = -1$). The only constraint on the three phases Φ_A, Φ_B and Φ_C is that they must sum to $\Psi - \Phi_S$. As discussed in McFadden *et al.* (1988), depending on the value of Ψ, these solutions have a three-fold symmetry, but not necessarily a six-fold symmetry; we shall discuss this point in more detail below.

A linear stability analysis of the bifurcating solution in which both the amplitude and phase of the solutions are perturbed shows that these solutions are unstable: the supercritical solution branch is amplitude-unstable to two normal modes and phase-unstable to another, and the subcritical solution branch is amplitude-unstable to a single normal mode.

Following Brattkus & Davis (1988), stable solution branches can be found through a higher-order analysis in the case that the quadratic coefficient λ is small; this requires the distribution coefficient to be near unity and the anisotropy coefficient $\hat{\gamma}_3$ to be small. In this case, third-order terms must be included in the amplitude equations.

When the orientation of the pattern is such that $\cos 3\psi = 0$, these equations are identical to those considered by Brattkus & Davis (1988). When $\cos 3\psi \neq 0$, we have

$$0 = sR_A + \lambda R_B R_C \mathrm{e}^{\mathrm{i}\Phi_S} - \tfrac{1}{2} R_A \{R_A^2 + \tfrac{3}{2}(R_B^2 + R_C^2)\}, \tag{6.21}$$

for steady-state solutions. Two other equations obtained by cyclic permutation of the subscripts $\{A, B, C\}$ also hold. The effect of the anisotropy is contained in the phase Ψ that appears in the term Φ_S. The formal structure of the steady-state equations is therefore unaltered by the addition of anisotropy in this approximation, and the corresponding bifurcation diagram, shown in figure 5, is equivalent to that shown by fig. 8 of Brattkus & Davis (1988). For example, rolls bifurcate supercritically, and the roll described, say, by $R_A^2 = 2s$, with $R_B = R_C = 0$, is unstable at small amplitudes, and regains stability for $R_A > 4\lambda$ ($s > 8\lambda^2$). The solutions considered above with $R_A = R_B = R_C \neq 0$ again bifurcate transcritically, and the subcritical branch reaches a limit point with $R_A = \lambda/4$ for $s = -\lambda^2/8$, and, for larger amplitudes, is stable until it loses stability for $R_A > 4\lambda$ ($s > 28\lambda^2$). (This change in stability is due to a secondary bifurcation of the unstable mixed-mode solution (Segel & Stuart 1962), which is also responsible for the stability change of the roll solutions.) The effect of anisotropy enters through the numerical value of λ, which increases monotonically with the magnitude of $\hat{\gamma}_3 \cos 3\psi$; as $|\hat{\gamma}_3 \cos 3\psi|$ increases, the range of stable rolls decreases, and the range of stable solutions with $R_A = R_B = R_C \neq 0$ increases. We note that even for $\hat{\gamma}_3 \neq 0$, if the orientation of the pattern is such that $\cos 3\psi = 0$, the anisotropy has no effect and the isotropic solution results.

As described in McFadden *et al.* (1988), the solutions with $R_A = R_B = R_C \neq 0$ represent hexagons with six-fold symmetry for $\Psi = 0$; the stable branch corresponds to solute distributions that are denoted (Morris & Winegard 1969) as 'nodes'. For $0 < \Psi < \pi/2$, the stable solutions with $R_A = R_B = R_C \neq 0$ have three-fold but not six-fold symmetry, and for $\Psi = \pi/2$, the interfacial pattern is triangular; examples are shown in figure 10.

7. Growth in the [011] direction: linear selection by anisotropy

When growth is in the [011] direction, anisotropy causes the linear growth rate of disturbances to be dependent upon their orientation. As a result, rolls aligned along one of the two symmetry axes are selected close to the onset of instability.

PHILOSOPHICAL TRANSACTIONS OF THE ROYAL SOCIETY A MATHEMATICAL, PHYSICAL & ENGINEERING SCIENCES

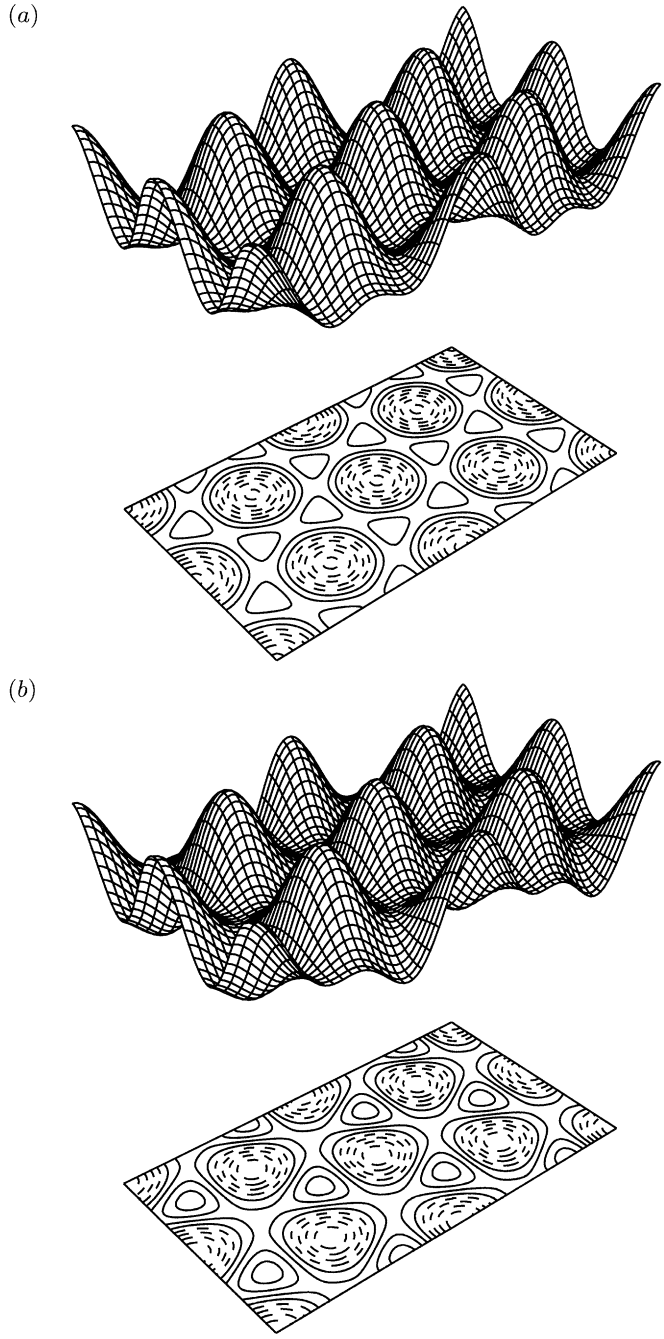

Figure 10. Effect of anisotropy on interface shape for growth in the [111] direction. The diagrams show a surface plot of the scaled interface position, $F = \delta\{A\mathrm{e}^{\mathrm{i}a(\xi\cos\psi+\eta\sin\psi)} + B\mathrm{e}^{\mathrm{i}a\{\xi\cos(\psi+2\pi/3)+\eta\sin(\psi+2\pi/3)\}} + C\mathrm{e}^{\mathrm{i}a\{\xi\cos(\psi-2\pi/3)+\eta\sin(\psi-2\pi/3)\}} + \text{c.c.}\}$, where $A = R_A\mathrm{e}^{\mathrm{i}\Phi_A}$, $B = R_B\mathrm{e}^{\mathrm{i}\Phi_B}$ and $C = R_C\mathrm{e}^{\mathrm{i}\Phi_C}$, with a contour plot projected onto a horizontal plane below. We take $R_A = R_B = R_C = 0.05$ and $\Phi_A = \Phi_B = \Phi_C = \Psi/3$, corresponding to the solution branch with $\Phi_S = \Psi - (\Phi_A + \Phi_B + \Phi_C) = 0$; here Ψ is a phase angle determined by the degree of anisotropy; (*a*) $\Psi = 0$, (*b*) $\Psi = \pi/4$, and (*c*) $\Psi = \pi/2$.

(*c*)

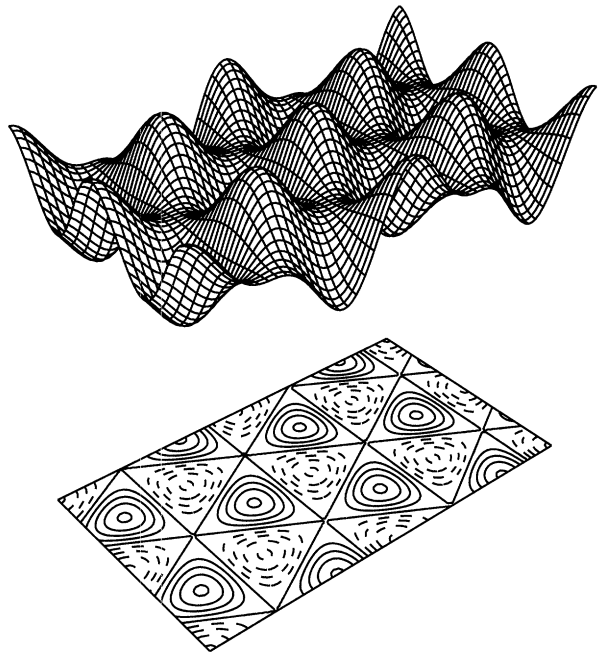

Figure 10. *Cont.*

(*a*) *Roll/rectangle competition*

Roll/rectangle competition is governed by the equations

$$a^2 A_T = (s - s_1)A - \alpha_1 |A|^2 A - \alpha_2 |B|^2 A, \tag{7.1a}$$

$$a^2 B_T = (s - s_2)B - \beta_1 |B|^2 B - \beta_2 |A|^2 B, \tag{7.1b}$$

where

$$s_1 = \frac{2\nu\hat{\gamma}_2 a^2}{1-\nu}\sin^2\psi, \tag{7.2a}$$

$$s_2 = \frac{2\nu\hat{\gamma}_2 a^2}{1-\nu}\sin^2(\psi+\theta), \tag{7.2b}$$

$$\alpha_1 = \tfrac{8}{9}a^6 + 12a^4\gamma_4 + 12a^4\sin^2\psi[(\gamma_6-\gamma_4)\sin^2\psi + (\gamma_5 - 2\gamma_4)\cos^2\psi], \tag{7.2c}$$

$$\beta_1 = \tfrac{8}{9}a^6 + 12a^4\gamma_4 + 12a^4\sin^2(\psi+\theta) \times[(\gamma_6-\gamma_4)\sin^2(\psi+\theta) + (\gamma_5-2\gamma_4)\cos^2(\psi+\theta)], \tag{7.2d}$$

$$\begin{aligned}\alpha_2 = \beta_2 = {} & \frac{8a^6}{(1-4\cos^2\theta)^2}[\nu(1-2\nu) - (2-5\nu+4\nu^2)\cos^2\theta \\ & +2(2-7\nu+7\nu^2)\cos^4\theta + 8\nu(1-\nu)\cos^6\theta] \\ & +8a^4\gamma_4(1+2\cos^2\theta) \\ & +2a^4(\gamma_5-2\gamma_4)[2\sin^2(2\psi+\theta) + \sin(2\psi+2\theta)\sin 2\psi] \\ & +24a^4(\gamma_6-\gamma_4)\sin^2\psi\sin^2(\psi+\theta).\end{aligned} \tag{7.2e}$$

In the isotropic case, we have $\hat{\gamma}_2 = 0$, $\gamma_5 = 2\gamma_4 = 2\gamma_6 = -\frac{1}{4}$ (McFadden *et al.* 1988). Anisotropy leads to different linear growth rates for the A and B rolls; in other

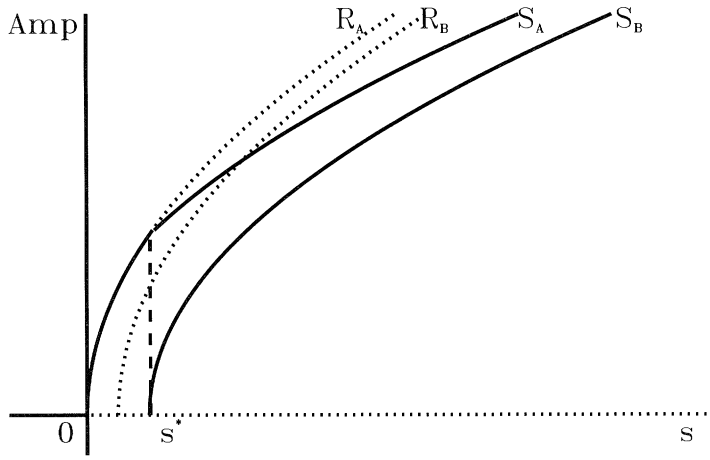

Figure 11. Bifurcation diagram for rectangles in the [110] case. The amplitudes of the two component rolls, labelled R_A and R_B, are plotted against s, along with the amplitudes of the two rectangle components, labelled S_A and S_B. The curves labelled R_A and S_A actually lie in a plane perpendicular to that containing the curves labelled R_B and S_B, although they are drawn against the same axes here for convenience. Consequently, it should be borne in mind that the curves R_B and S_A do not actually meet. Unstable solutions are indicated by dotted curves, and stable branches by solid curves.

words, we have $s_1 \neq s_2$. There are also changes in the cubic coefficients, although all remain purely real.

(i) *Summary of the effects of anisotropy on roll and rectangle solutions*

In contrast to the isotropic case, where both roll and rectangle solution branches bifurcate from the trivial solution at the origin ($A = B = s = 0$), we shall see that in the presence of anisotropy, the rectangles bifurcate from one of the roll solutions, and each set of rolls bifurcates separately from the trivial solution (figure 11). Close to onset, we find only roll solutions, as expected from the linear analysis; the anisotropy favours rolls that are aligned along one or other of the symmetry axes according to the sign of $\hat{\gamma}_2$. Far from onset, the linear effects of anisotropy are less noticeable, and the changes in the existence and stability requirements for steady solutions are influenced primarily by anisotropy at cubic order; this situation is very similar to that of growth in the [100] case, and the general stability results summarized in § 5 *a* (i) hold with the new definitions of α_1, β_1 and α_2.

(ii) *Existence and stability requirements for roll and rectangle solutions*

The trivial solution $A = B = 0$ is stationary, as are A rolls

$$|A|^2 = (s - s_1)/\alpha_1, \quad B = 0, \tag{7.3}$$

and B rolls

$$|B|^2 = (s - s_2)/\beta_1, \quad A = 0. \tag{7.4}$$

Rectangles

$$|A|^2 = \frac{[s(\beta_1 - \alpha_2) - (\beta_1 s_1 - \alpha_2 s_2)]}{\alpha_1\beta_1 - \alpha_2^2}, \quad |B|^2 = \frac{[s(\alpha_1 - \alpha_2) - (\alpha_1 s_2 - \alpha_2 s_1)]}{\alpha_1\beta_1 - \alpha_2^2} \tag{7.5}$$

are another steady solution.

A rolls bifurcate supercritically if $\alpha_1 > 0$, and subcritically otherwise. They are stable for $s > s_1$ and $s - s_2 - \alpha_2(s - s_1)/\alpha_1 < 0$, and unstable otherwise. B rolls bifurcate supercritically if $\beta_1 > 0$, subcritically otherwise, and are stable for $s > s_2$ and $s - s_1 - \alpha_2(s - s_2)/\beta_1 < 0$, unstable otherwise. If $\hat{\gamma}_2 > 0$, then whichever set of rolls has its axes more nearly aligned along the η axis bifurcates from the zero solution first (i.e. at a lower value of s). However, if $\hat{\gamma}_2 < 0$, then the set of rolls whose axes are more nearly aligned along the ξ axis bifurcates first. In both cases, if this set of rolls bifurcates supercritically, then it is also the stable solution near onset. In other words, linear selection picks rolls aligned in the direction that maximizes their growth rate.

Rectangles exist for

$$s > \max\left[\frac{\beta_1 s_1 - \alpha_2 s_2}{\beta_1 - \alpha_2}, \frac{\alpha_1 s_2 - \alpha_2 s_1}{\alpha_1 - \alpha_2}\right] \quad \text{if } q_1 > 0,\ q_2 > 0, \tag{7.6}$$

$$\frac{\beta_1 s_1 - \alpha_2 s_2}{\beta_1 - \alpha_2} < s < \frac{\alpha_1 s_2 - \alpha_2 s_1}{\alpha_1 - \alpha_2} \quad \text{if } q_1 > 0,\ q_2 < 0, \tag{7.7}$$

$$\frac{\alpha_1 s_2 - \alpha_2 s_1}{\alpha_1 - \alpha_2} < s < \frac{\beta_1 s_1 - \alpha_2 s_2}{\beta_1 - \alpha_2} \quad \text{if } q_1 < 0,\ q_2 > 0, \tag{7.8}$$

$$s < \min\left[\frac{\beta_1 s_1 - \alpha_2 s_2}{\beta_1 - \alpha_2}, \frac{\alpha_1 s_2 - \alpha_2 s_1}{\alpha_1 - \alpha_2}\right] \quad \text{if } q_1 < 0,\ q_2 < 0, \tag{7.9}$$

where

$$q_1 = \frac{\beta_1 - \alpha_2}{\alpha_1\beta_1 - \alpha_2^2}, \quad q_2 = \frac{\alpha_1 - \alpha_2}{\alpha_1\beta_1 - \alpha_2^2}. \tag{7.10}$$

They are stable if $\alpha_1 > 0$, $\beta_1 > 0$ and $\alpha_1\beta_1 > \alpha_2^2$.

The rectangles do not bifurcate from the origin ($A = B = s = 0$), owing to the different linear growth rates of the constituent rolls. One of the rectangle components bifurcates from one of the roll branches, and the other component bifurcates from zero at the same value of the bifurcation parameter. For example, if $q_1 > 0$, $q_2 > 0$ and $(\alpha_1 s_2 - \alpha_2 s_1)/(\alpha_1 - \alpha_2) > (\beta_1 s_1 - \alpha_2 s_2)/(\beta_1 - \alpha_2)$, then for $s < s_* = (\alpha_1 s_2 - \alpha_2 s_1)/(\alpha_1 - \alpha_2)$, there are no rectangles, because the relevant S_0^2 is negative. At $s = s_*$, the A roll branch and the A component of the rectangle branch meet. In other words, the A component of the rectangles branches off from the A rolls, and the B component of the rectangles bifurcates from zero at $s = s_*$. So close to onset, there are only roll solutions, as expected from the linear analysis. Figure 11 shows the bifurcation diagram in the case $s_2 > s_1$, $\alpha_1 > 0$, $\beta_1 > 0$, $\alpha_1\beta_1 > \alpha_2^2$.

(*b*) *Roll/hexagon competition*

Hexagon/roll competition is governed by the equations

$$\begin{aligned} a^2 A_T = {} & [s - \hat{s}(\psi)]A + \alpha\bar{B}\bar{C} - \mu_1(\psi)|A|^2 A - \mu_2(\psi)|B|^2 A \\ & - \mu_2(\psi - 2\pi/3)|C|^2 A, \end{aligned} \tag{7.11a}$$

$$\begin{aligned} a^2 B_T = {} & [s - \hat{s}(\psi + 2\pi/3)]B + \alpha\bar{A}\bar{C} - \mu_1(\psi + 2\pi/3)|B|^2 B \\ & - \mu_2(\psi + 2\pi/3)|C|^2 B - \mu_2(\psi)|A|^2 B, \end{aligned} \tag{7.11b}$$

$$\begin{aligned} a^2 C_T = {} & [s - \hat{s}(\psi - 2\pi/3)]C + \alpha\bar{A}\bar{B} - \mu_1(\psi - 2\pi/3)|C|^2 C \\ & - \mu_2(\psi - 2\pi/3)|A|^2 C - \mu_2(\psi + 2\pi/3)|B|^2 C, \end{aligned} \tag{7.11c}$$

where

$$\hat{s}(\phi) = \frac{2\nu\hat{\gamma}_2 a^2}{1-\nu}\sin^2\phi, \tag{7.12a}$$

$$(= \hat{\gamma}_2 a^2 \sin^2\phi,) \tag{7.12b}$$

$$\alpha = (1-3\nu)a^4/2, \tag{7.12c}$$

$$\mu_1(\phi) = 2a^4 + 12a^4\gamma_4 + 12a^4\sin^2\phi[(\gamma_6-\gamma_4)\sin^2\phi + (\gamma_5-2\gamma_4)\cos^2\phi], \tag{7.12d}$$

$$\mu_2(\phi) = \tfrac{9}{4}a^4 + 12a^4\gamma_4 + 2a^4(\gamma_5-2\gamma_4)[2\sin^2(2\phi+2\pi/3) + \sin 2\phi\sin(2\phi-2\pi/3)] + 24a^4(\gamma_6-\gamma_4)\sin^2\phi\sin^2(\phi+2\pi/3). \tag{7.12e}$$

If $|1-3\nu|$ is of unit order, the equations must be truncated at second order, whereas if $3\nu \sim 1$, cubic terms must be included. The coefficients of the cubic terms given above are appropriate when $|1-3\nu|$ is small (recall that we then have $a^2 = 9/4$). In this case, the coefficients of the linear terms are also affected. The first expression given for $\hat{s}$ is for general ν, while the expression in brackets holds for the case $3\nu \sim 1$ small, when cubic terms are included. In the isotropic case, we have $\hat{\gamma}_2 = 0$, i.e. $\hat{s}(\phi) \equiv 0$, and $\gamma_5 = 2\gamma_4 = 2\gamma_6 = -\frac{1}{4}$ (McFadden *et al.* 1988). Anisotropy results in the A, B and C rolls all having different linear growth rates, and also changes the coefficients of the cubic terms, although the quadratic coefficients are unchanged.

(i) *Summary of the effects of anisotropy on hexagonal solutions*

The anisotropy appears here at linear order; the linear growth rates of the three sets of rolls are all different. Consequently, the three rolls bifurcate from the trivial solution separately, and the hexagons do not bifurcate from the origin, as they would in the isotropic case (figure 5). As in the case of roll/rectangle competition, rolls aligned along one or other of the symmetry axes are favoured. We shall see that hexagonal nodes bifurcate from the leftmost roll branch, and cells from the rightmost (figure 12). Far from the origin, the bifurcation structure is the similar to that in the [100] case. Again, there is no clear distinction between mixed mode and hexagon-type solutions, owing to the effect of anisotropy on the cubic coefficients.

(ii) *Bifurcation structure for hexagonal solutions*

Hexagons do not bifurcate from the origin, since the linear growth rates of the three sets of rolls are unequal. Note that the leftmost roll branch is once again that which is most nearly aligned along the η axis if $\hat{\gamma}_2 > 0$, and that most nearly aligned along the ξ axis if $\hat{\gamma}_2 < 0$. In addition, we shall see below that if it bifurcates supercritically from the zero solution, it is stable at onset; the anisotropy linearly selects rolls aligned along one or other of the symmetry axes.

A simplified notation will be used here; we shall write $s_1 = \hat{s}(\psi)$, $s_2 = \hat{s}(\psi+2\pi/3)$, $s_3 = \hat{s}(\psi-2\pi/3)$, $\mu_1 = \mu_1(\psi)$, $\mu_2 = \mu_2(\psi)$ and $\mu_3 = \mu_2(\psi-2\pi/3)$. A linear stability analysis of the A roll solution $A = R_0$, $R_0^2 = (s-s_1)/\mu_1$, $B = C = 0$, shows that the rolls are stable if

$$s > s_1, \tag{7.13a}$$

$$2s - s_2 - s_3 - (\mu_2+\mu_3)R_0^2 < 0, \tag{7.13b}$$

$$(s-s_2)(s-s_3) - (s-s_3)\mu_2 R_0^2 - (s-s_2)\mu_3 R_0^2 + \mu_2\mu_3 R_0^4 - \alpha^2 R_0^2 > 0. \tag{7.13c}$$

Consequently, if $s_1 < s_2$, $s_1 < s_3$, so that the A roll branch is the leftmost, and if it bifurcates supercritically, so that $s > s_1$, then the A rolls are stable at onset.

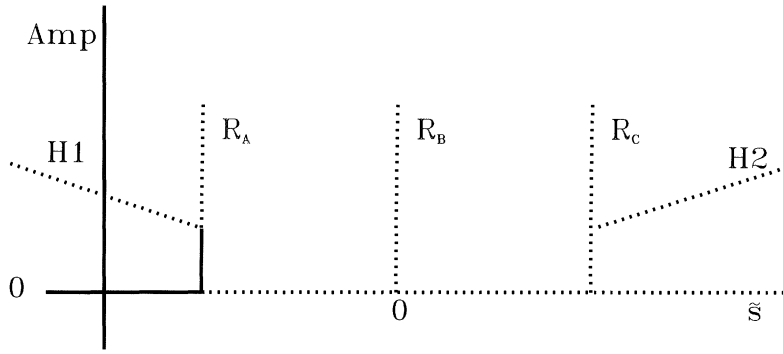

Figure 12. Schematic bifurcation diagram for hexagons in the [110] case. A region close to the origin is depicted. The amplitudes of all three component rolls, labelled R_A, R_B and R_C, are plotted against $\tilde{s}$, along with the amplitudes of the hexagonal nodes (labelled H1) and the hexagonal cells (labelled H2). Unstable solution branches are indicated by dotted curves, and stable branches by solid curves. Close to the origin, both hexagonal nodes and cells are unstable, but far away from the origin, the node branch is expected to turn around, and become stable.

There are two bifurcation points on the roll solution, where the linear growth rate of perturbations is zero, one at each of the values of s which are the roots of the equation

$$\begin{aligned} &s^2(\mu_1^2 - \mu_1\mu_2 - \mu_1\mu_3 + \mu_2\mu_3) \\ &\quad + s(-s_2\mu_1^2 - s_3\mu_1^2 + \mu_1\mu_2 s_3 + \mu_1\mu_2 s_1 + \mu_1\mu_3 s_1 + \mu_1\mu_3 s_2 - 2\mu_2\mu_3 s_1 - \mu_1\alpha^2) \\ &\quad + (\mu_1^2 s_2 s_3 - \mu_1\mu_2 s_1 s_3 - \mu_1\mu_3 s_1 s_2 + \mu_1\alpha^2 s_1 + \mu_2\mu_3 s_1^2) = 0. \end{aligned} \tag{7.14}$$

In the isotropic limit, where $s_1 = s_2 = s_3 = 0$, and $\mu_3 = \mu_2$, the roots to this equation are given by $s = 0$ and $s = \mu_1\alpha^2/(\mu_1 - \mu_2)^2$, the latter being the position of the bifurcation to mixed modes, and the former being the position of the primary bifurcation, to rolls and hexagons. If $s_i - s_j$ is small, we find that the $s = 0$ root moves to $s = s_1 + \tilde{s}$, where $\tilde{s} = \mu_1(s_1 - s_2)(s_1 - s_3)/\alpha^2 + O(\{s_i - s_j\}^3)$. The bifurcation point lies on the branch of roll solutions if $R_0^2 = (s_1 - s_2)(s_1 - s_3)/\alpha^2 > 0$, i.e. if $s_1 < \min(s_2, s_3)$ or $s_1 > \max(s_2, s_3)$. So this bifurcation point occurs on the leftmost and the rightmost of the three roll solution branches, but not on the middle branch. If the real perturbations to the roll amplitude are written in the form $A = R_0(1 + r)$, $B = R_0 b$, and $C = R_0 c$, where $|r|, |b|, |c| \ll 1$, then at the bifurcation point, the perturbation eigenvector corresponding to the zero growth rate eigenvalue is given by $r = 0$ and $b = -\{|s_1 - s_3|^{1/2}/|s_1 - s_2|^{1/2}\}c$ if $s_1 > \max(s_2, s_3)$, or $b = \{|s_1 - s_3|^{1/2}/|s_1 - s_2|^{1/2}\}c$ if $s_1 < \min(s_2, s_3)$. This suggests that 'nodes' bifurcate from the leftmost roll branch, and 'cells' from the rightmost. Malomed *et al.* (1994) also found that hexagonal nodes bifurcate from one of the roll branches when the linear growth rates are unequal, and that there is a change in stability of the roll at that point.

The second root moves to $s = s_1 + \tilde{s}$, where $\tilde{s} = \mu_1\alpha^2/(\mu_1 - \mu_2)(\mu_1 - \mu_3) + O(s_i - s_j)$. If we write $s = s_1 + \tilde{s}$ in the amplitude equations (7.11 *a*), (7.11 *b*) and (7.11 *c*), and assume that $s_i - s_j$ is small in comparison with $\tilde{s}$, we find a similar situation to the [100] case, except that s is replaced by $\tilde{s}$, and the precise form of the cubic coefficients differs. So for large $\tilde{s}$, the bifurcation structure is similar to that in the [100] case,

and we can assume that a branch of mixed mode solutions bifurcates from the roll branch at $\tilde{s} = \mu_1\alpha^2/(\mu_1 - \mu_2)(\mu_1 - \mu_3)$.

Close to the beginning of the roll branch, where R_0 is small, the growth rates of real perturbations are $\sigma_1 = -2\mu_1 R_0^2$, $\sigma_2 = s_1 - s_2$ and $\sigma_3 = s_1 - s_3$. Thus, assuming $\mu_1(\psi)$, $\mu_1(\psi + 2\pi/3)$ and $\mu_1(\psi - 2\pi/3)$ are all positive, the leftmost roll branch has three negative eigenvalues at onset, the middle branch two negative eigenvalues, and the rightmost has only one negative eigenvalue. Far from onset, in the case $\mu_1 > 0$, $\mu_1 - \mu_2 < 0$ and $\mu_1 - \mu_3 < 0$, the roll branch has two negative eigenvalues if $\tilde{s} < s_* \equiv \alpha^2\mu_1/(\mu_1 - \mu_2)(\mu_1 - \mu_3)$, and three if $\tilde{s} > s_*$. Taking into account the bifurcations to hexagons, we find that the leftmost roll has three negative eigenvalues for

$$0 < \tilde{s} < \frac{\mu_1(s_1 - s_2)(s_1 - s_3)}{\alpha^2},$$

then two for

$$\frac{\mu_1(s_1 - s_2)(s_1 - s_3)}{\alpha^2} < \tilde{s} < \frac{\alpha^2\mu_1}{(\mu_1 - \mu_2)(\mu_1 - \mu_3)}$$

and three for

$$\tilde{s} > \frac{\alpha^2\mu_1}{(\mu_1 - \mu_2)(\mu_1 - \mu_3)}.$$

The middle roll has two negative eigenvalues for

$$0 < \tilde{s} < \frac{\alpha^2\mu_1}{(\mu_1 - \mu_2)(\mu_1 - \mu_3)},$$

and three for

$$\tilde{s} > \frac{\alpha^2\mu_1}{(\mu_1 - \mu_2)(\mu_1 - \mu_3)}.$$

The rightmost roll has one negative eigenvalue for

$$0 < \tilde{s} < \frac{\mu_1(s_1 - s_2)(s_1 - s_3)}{\alpha^2},$$

two for

$$\frac{\mu_1(s_1 - s_2)(s_1 - s_3)}{\alpha^2} < \tilde{s} < \frac{\alpha^2\mu_1}{(\mu_1 - \mu_2)(\mu_1 - \mu_3)},$$

and three for

$$\tilde{s} > \frac{\alpha^2\mu_1}{(\mu_1 - \mu_2)(\mu_1 - \mu_3)}.$$

Again, we have assumed that $\mu_1(\psi)$, $\mu_1(\psi + 2\pi/3)$ and $\mu_1(\psi - 2\pi/3)$ are all positive.

The hexagonal nodes are unstable when they bifurcate from the leftmost roll, having one positive eigenvalue. The hexagonal cells are also unstable, having two positive eigenvalues. Figure 12 shows a region of the bifurcation diagram close to the origin. Far from the origin, the system approaches the behaviour which would be expected in the case $\hat{s}(\phi) \equiv 0$, which is very similar to the [100] case.

Here, as in the [100] case, there is no longer a clear distinction between mixed mode and hexagon-type solutions, owing to the effect of anisotropy on the cubic coefficients. In fact, for the case $\psi = 0$, when one of the rolls is aligned along the η axis, the bifurcation structure is exactly the same as given by equations (5.15) in the [100] case if we now redefine $-\lambda_2 = (81a^4/4)(\gamma_6 - \gamma_4) - (9a^4/4)(\gamma_5 - 2\gamma_4)$. An

PHILOSOPHICAL TRANSACTIONS OF THE ROYAL SOCIETY A MATHEMATICAL, PHYSICAL & ENGINEERING SCIENCES

analysis for small ψ reveals that in the [011] case, the equivalent of equations (5.20) is

$$\left.\begin{aligned} r &= O(\psi^2), \\ b = -c &= \frac{3\sqrt{3}a^4\psi\{[-3(\gamma_6-\gamma_4)+(\gamma_5-2\gamma_4)]R_B^2-2(\gamma_5-2\gamma_4)R_A^2\}}{2[-\alpha R_A+(a^4/4)\{1+27(\gamma_6-\gamma_4)-15(\gamma_5-2\gamma_4)\}R_B^2]}. \end{aligned}\right\} \tag{7.15}$$

Again, as ψ increases slightly from zero, the B and C roll amplitudes split away from each other symmetrically, while the A roll amplitude remains constant. The imperfect bifurcation structure for the $\psi = 0$ case is embedded in the general ψ case.

8. Discussion

In many physical systems (e.g. liquid crystals, directional solidification, convection between thermally anisotropic plates (Pearlstein & Oztekin 1989)), the materials of interest possess intrinsic anisotropies that select certain directions as preferred. These geometrical constraints offer strong preferences for pattern selection. In an effort to investigate the competition between the pattern selected by nonlinearity and that intrinsic to the geometry, surface-energy anisotropy is allowed in a model of directional solidification. This model is valid near the upper (absolute stability) branch of the morphological instability neutral curve where, in the isotropic case, bifurcation in two dimensions is supercritical. This model ignores the effects of thermodynamic disequilibrium that would be present at high speeds in standard metallic or organic alloys. We expect the results that we obtain from consideration of surface-tension anisotropy to be typical of other types of anisotropic properties as well, since the various anisotropic properties of the solid are all determined by the basic symmetries of the underlying crystal lattice.

The anisotropy selected is surface energy in cubic crystals. Thus, for growth in the [100] direction there is four-fold symmetry, for [111] growth a three-fold symmetry, and for [011] growth a two-fold symmetry. Consequently, the plane on which patterns evolve has intrinsic preferred directions. These symmetries suggest the consideration of roll/rectangle and roll/hexagon competitions.

The starting point is the limit of near absolute stability in which Brattkus & Davis (1988) derived an asymptotically correct evolution equation that represents the full free-boundary problem of the strongly nonlinear morphological instability. This equation is generalized to the cases of cubic anisotropy, with growth in the [100], [111] or [110] directions. From these partial differential equations, systems of ordinary differential equations are derived in the weakly nonlinear limit. These amplitude equations are of the usual type standard in, say, Bénard convection except that the coefficients inherit asymmetries from the surface energy. Analysis of these equations gives insights into the formerly described competitions.

For growth in the [100] direction, the anisotropy enters the amplitude equations only in the cubic coefficients; all coefficients are real. The competition between rolls and rectangles is shown in figures 6–8. The analysis predicts for the isotropic case, that whether squares or rolls are to be preferred depends on the value of the distribution coefficient, k. For k near unity, rolls are preferred over squares, and there is an exchange of preference for sufficiently large departures of k from unity. When anisotropy is present, rectangles can lose existence, one roll can be stable while the other loses stability, or rolls and rectangles can all be unstable locally.

Roughly square-shaped patterns of solute segregation were observed by Flemings *et al.* (1970) during directional solidification of Fe–10% Ni alloys. The observed four-fold symmetry of the patterns is likely associated with the incipient formation of sidearms during the cell/dendrite transition, but the observed arrangement of the cells into a square array is suggestive even if the growth is probably occurring well past the onset of instability considered here.

The hexagon/roll competition in this case leads to various situations depending on the angle that the hexagon makes with the underlying preferred directions. When aligned, $\psi = 0$, there is a loss of distinction between hexagons and other mixed modes. Hence, the loss of symmetry induces imperfections in the secondary bifurcations (see Tilley *et al.* (1994) for another such case). Whereas a mixed mode ('Class V') crosses the hexagon mode in the isotropic case, figure 9*a*, anisotropy breaks this bifurcation, as shown in figures 9*b*, *c*. When $\psi = 0$, two of the three rolls have equal amplitudes for all values of the bifurcation parameter. For small misalignments, $0 < |\psi| \ll 1$, however, these two roll amplitudes split apart symmetrically from their $\psi = 0$ values.

For growth in the [111] direction, the anisotropy enters the amplitude equations in the quadratic coefficients, which are complex. In the roll/rectangle competition the usual two supercritical rolls can change to both subcritical or one of each. Further, the complex coefficients result in some rolls or rectangles travelling.

The hexagon/roll competition in this case leads to various possibilities. There can be six-fold symmetry, three-fold but not six-fold symmetry, or triangular symmetry depending on the orientation to the crystalline axes, the degree of anisotropy, and the distribution coefficient.

For growth in the [110] direction, the anisotropy enters the amplitude equations in the linear and cubic coefficients; the coefficients are real. The competition between rolls and rectangles is shown in figure 11. Since the growth rates are angle-dependent, the two rolls bifurcate at different values of s. The rectangles now bifurcate from the first roll to exist. Far from onset, the linear selection is weak and the cubic coefficients dominate the selection process, which now resembles that of the [100] case.

The hexagon/roll competition in this case is shown in figure 12. The linear selection splits the degeneracy of the rolls so that all three bifurcate at different values of s. Hexagonal nodes bifurcate from the leftmost roll, while hexagonal cells bifurcate from the rightmost roll. Again, mixed modes and hexagons become indistinguishable. In the example shown, all hexagonal states are unstable close to the origin, but at large amplitudes, the hexagonal node branch will turn around becoming stable, and the situation is similar to that in the [100] case (figure 9).

The present study gives a variety of cases in which the intrinsic asymmetry, in this case surface energy, competes with selection by nonlinearity.

The authors are grateful for helpful discussions with Dr R. J. Braun and Dr S. R. Coriell. This work was partly supported by a grant from NASA Microgravity Science and Applications Program, and by the Applied and Computational Mathematics Program of ARPA.

References

Brattkus, K. & Davis, S. H. 1988 *Phys. Rev.* B **38**, 11452.

Busse, F. H. 1967 *J. Fluid Mech.* **30**, 625.

Coriell, S. R. & McFadden, G. B. 1993 In *Handbook of crystal growth* (ed. D. T. J. Hurle), vol. 1, Part B, pp. 785–857. Amsterdam: North Holland.

Coriell, S. R. & Sekerka, R. F. 1976 *J. Crystal Growth* **34**, 157.

PHILOSOPHICAL TRANSACTIONS OF THE ROYAL SOCIETY A MATHEMATICAL, PHYSICAL & ENGINEERING SCIENCES

Coriell, S. R., McFadden, G. B. & Sekerka, R. F. 1990 *J. Crystal Growth* **100**, 459.

de Cheveigné, S., Guthmann, C., Kurowski, P., Vicente, E. & Biloni, H. 1988 *J. Crystal Growth* **92**, 616.

Dougherty, A. 1991 *J. Crystal Growth* **110**, 501.

Flemings, M. C., Poirier, D. R., Barone, R. V. & Brody, H. D. 1970 *J. Iron Steel Inst.* **208**, 371.

Glicksman, M. E. & Singh, N. B. 1986 In *Rapidly solidified powder aluminum alloys* (ed. M. E. Fine & E. A. Stark Jr), p. 44. Philadelphia: ASTM.

Glicksman, M. E. & Singh, N. B. 1989 *J. Crystal Growth* **98**, 277.

Golubitsky, M. & Schaeffer, D. G. 1985 *Singularities and groups in bifurcation theory*, p. 434. New York: Springer.

Herring, C. 1951 In *Lectures of powder metallurgy* (ed. R. E. Kingston), p. 143. New York: McGraw-Hill.

Hoyle, R. B. 1993 *Physica* D **67**, 198.

Hoyle, R. B., McFadden, G. B. & Davis, S. H. 1995 Applied Mathematics Technical Report no. 9404, Northwestern University.

Huntley, D. A. & Davis, S. H. 1993 *Acta Metall. Mater.* **41**, 2025.

Joets A. & Ribotta, R. 1988 *J. Phys. (Paris)* **47**, 595.

Kai, S. & Hirakawa, K. 1978 *Prog. Theor. Phys. Suppl.* **64**, 212.

Langer, J. S. 1987 In *Chance and matter* (ed. J. Souletie, J. Vannimenus & R. Stora). Lectures on the Theory of Pattern Formation, Les Houches Summer School, 1986. Amsterdam: North-Holland.

McFadden, G. B., Coriell, S. R. & Sekerka, R. F. 1988 *J. Crystal Growth* **91**, 180.

Malomed, B. A., Nepomnyashchy, A. A. & Nuz, A. E. 1994 *Physica* D **70**, 357.

Morris, L. R. & Winegard, W. C. 1969 *J. Crystal Growth* **5**, 361.

Mullins, W. W. & Sekerka, R. F. 1964 *J. Appl. Phys.* **35**, 444.

Muschol, M., Liu, D. & Cummins, H. Z. 1992 *Phys. Rev.* A **46**, 1038.

Pearlstein, A. J. & Oztekin, A. 1989 *J. Fluid Mech.* **207**, 267.

Segel, L. A. & Stuart, J. T. 1962 *J. Fluid Mech.* **13**, 289.

Taylor, J. E. 1992 *Acta Metall. Mater.* **40**, 1475.

Tilley, B. S., Davis, S. H. & Bankoff, S. G. 1994 *J. Fluid Mech.* **277**, 55.

Voorhees, P. W., Coriell, S. R., McFadden, G. B. & Sekerka, R. F. 1984 *J. Crystal Growth* **67**, 425.

Wollkind, D. J. & Segel, L. A. 1970 *Phil. Trans. R. Soc. Lond.* A **268**, 351.

Young, G. W., Brattkus, K. & Davis, S. H. 1987 *J. Crystal Growth* **83**, 560.

Received 18 January 1995; revised 5 September 1995; accepted 22 January 1996

PHILOSOPHICAL TRANSACTIONS OF THE ROYAL SOCIETY A MATHEMATICAL, PHYSICAL & ENGINEERING SCIENCES